1-7-93
7370

Unsteady Shear Disturbances Within a Two-Dimensional Stratified Flow

Jeffrey W. Yokota
Sverdrup Technology, Inc.
Lewis Research Center Group
Brook Park, Ohio

October 1992

NASA
National Aeronautics and
Space Administration

Unsteady Shear Disturbances Within a Two-Dimensional Stratified Flow

Jeffrey W. Yokota

Sverdrup Technology, Inc.

NASA Lewis Research Center Group

Brook Park, Ohio   44142

ABSTRACT

The origin and evolution of shear disturbances within a stratified, inviscid, incompressible flow are investigated numerically by a Clebsch/Weber decomposition-based scheme. In contrast to homogeneous flows, within which vorticity can be redistributed but not generated, the presence of a density stratification can render an otherwise irrotational flow vortical. In this work a kinematic decomposition of the unsteady Euler equations separates the unsteady velocity field into rotational and irrotational components. The subsequent evolution of these components is used to investigate the influence various velocity disturbances have on both stratified and homogenous flows.

In particular, the flow within a two-dimensional channel is used to investigate the evolution of rotational disturbances, generated or convected, downstream from an unsteady inflow condition. Contrasting simulations of both stratified and homogeneous flows are used to distinguish between redistributed inflow vorticity and that which is generated by a density stratification.

1. INTRODUCTION

The fluid dynamics of density stratifications, which commonly occur in atmospheric and oceanic flows, are of both practical and scientific interest. One significant difference between the behaviors of stratified and homogeneous flows is that vorticity can be generated by the presence

1

of a density gradient. More specifically, vorticity is generated when a pressure gradient exists perpendicular to the density stratification (Yih 1980).

Pressure gradients are often transient and vortical flows are usually unsteady; thus the need to understand and investigate unsteady flows becomes apparent. Unsteady flows in general, and transient vortical flows in particular, are often difficult to simulate either experimentally or numerically. However, as numerical techniques become increasingly accurate and efficient, they are being used to investigate flow phenomena of greater complexity. This is particularly true of vortical flows which have a significant impact on the flow around aircraft and through turbomachinery.

A kinematic description is an important, yet often neglected, approach to the understanding of vortical flows. The convection of material surfaces, a fundamental aspect of unsteady vortical flow, is rarely explored computationally. However, kinematic descriptions of steady vortical flows have proven fruitful, both analytically and numerically. General theories on the kinematics of vortical flow have been developed by Trusdell (1954) and Hawthorne (1966), while Yih (1960) introduced a transformation that, when coupled to Hawthorne's work, was used by Marris (1964) to study the generation of secondary vorticity in a stratified fluid. A Weber transformation was used by Goldstein (1978) to investigate weak velocity disturbances to the potential flow around arbitrary obstacles while Atassi and Scott (1988) extended this idea to the distortion of vortical waves as they convected past a series of thin airfoils. Recently the linking of a fluid element's displacement to its velocity change has been explored geometrically by Hunt and Hussain (1991), while the convection of material surfaces, an essential feature of any Clebsch transformation, forms the basis of Ottino's (1982) investigations into fluid mixing. Clearly, kinematic descriptions have proven valuable to the analytical investigation of vortical flow.

Clebsch potentials have also been used to simulate flows of applied aerodynamic interest, where the diffusion of vorticity, coupled with numerical economy, is of paramount concern. In most of these calculations, a vortical distortion is added to a steady potential flow; early exam-

ples of this approach include Murman and Stremel's (1982) wake simulation and Steinhoff and Suryanarayana's (1983) convecting vortex sheet. Grossman (1983) coupled a shock-fitting technique to a Clebsch potential scheme and calculated supersonic flows over a number of conical bodies. Lacor and Hirsch (1982) and Ecer and Akay (1983) have both simulated flows through turbomachinery while Chang and Adamczyk (1985a, 1985b) coupled Clebsch potentials to the Munk-Prim substitution principle and investigated the secondary flow in a turning channel. Although these and many other simulations were made tractable through a Clebsch decomposition, their application to unsteady flows has still not been widely exploited.

Initial conditions can dominate the evolution of an unsteady simulation and are unfortunately not a product of the Clebsch decomposition itself. This fact alone can be enough to discourage one from simulating an unsteady flow with an arbitrary Clebsch decomposition. However, an initial condition based on Lagrangian coordinates and the rotational component of the initial velocity field becomes apparent when a Clebsch decomposition is derived from the Weber transformation (Hunt 1987). While it may not be possible to construct a globally valid Clebsch decomposition for all times, the evolution of an initial transient should be simulated accurately. In the calculations that follow, both steady rotational and irrotational flows are constructed analytically, reproduced numerically, and then perturbed by a number of unsteady inflow velocity disturbances.

In the present work, the incompressible Euler equations are decomposed into scale elliptic and hyperbolic equations while the velocity field is separated into rotational and irrotational components. The rotational component is constructed from a series of complex-lamellar fields while the irrotational component is evaluated from a scalar potential field. By decomposing the velocity field into rotational and irrotational components, one can identify the origins of various shear disturbances. By knowing the transport equations that govern these components, one can determine how these disturbances are convected or propagated throughout the flow.

In each of the simulations to follow, a steady stratified flow is disrupted by velocity disturbances imposed at the inflow boundary. The interaction between these evolving velocity

disturbances and a statically stable density stratification is our primary interest. To allow these flows to evolve nonlinearly, both their rotational and irrotational velocity components are reconstructed during each time step of their unsteady simulation. Furthermore, the inflow density stratifications are held constant to avoid introducing a buoyancy drive disturbance or a Rayleigh-Taylor instability from the inflow boundary. Any displacement of the density interface results from an interaction with the evolving inflow velocity disturbances and is not explicitly imposed from the inflow boundary.

In the first series of calculations, a steady shear layer is perturbed by an oscillating inflow centerline. The disturbances that are generated by this forcing evolve into a series of nonlinear rollups that are only weakly affected by the presence of the density stratification. Consequently there is very little difference between the vortical structures present within the homogeneous and stratified flows.

The second series of calculations simulates the vortical disturbances generated by a starting inflow shear. Within these simulations, a vortex is generated at the leading edge of the shear layer, again attributed to the redistributed inflow shear, and again similar within both the homogeneous and stratified fluids. While the leading edge vortex is the primary rotational structure within these flows, a weaker downstream shear is generated within the stratified fluid. The shear generated downstream is quasi-two-dimensional in appearance and is both caused and controlled by the initial inflow velocity disturbances.

In the final series of calculations, an oscillating irrotational inflow is used to generate an unsteady shear within a stratified flow. In these simulations, an initially uniform, irrotational flow is forced by an oscillating irrotational inflow that renders the resulting flow both vortical and time-periodic. A series of spatially growing vortical structures created downstream of the inflow boundary simultaneously grow and diminish in time.

In each of the simulations to follow, a Clebsch/Weber decomposition of the velocity field is used to identify rotational disturbances and simulate their subsequent evolution. Within a

stratified fluid, vorticity can be convected, redistributed, or generated throughout the flow, and a Clebsch decomposition is used to identify and investigate each of these effects.

2. ANALYSIS

The incompressible Euler equations can be written in the Cartesian coordinate system (x, y) as

$$\frac{D\rho}{Dt} = 0 \qquad (1)$$

$$\frac{\partial u_i}{\partial x_i} = 0 \qquad (2)$$

$$\frac{Du_i}{Dt} = -\frac{1}{\rho} \frac{\partial p}{\partial x_i} - \frac{\partial}{\partial x_i} (gy) \qquad (3)$$

where (u, v) are the Cartesian velocity components, ρ is density, p is pressure, and g is gravitational acceleration. The material derivative is written

$$\frac{D}{Dt} = \frac{\partial}{\partial t} + u_j \frac{\partial}{\partial x_j} \qquad (4)$$

and Lagrangian coordinates (X, Y) satisfy

$$\frac{DX_i}{Dt} = 0 \qquad (5)$$

where the Cartesian/Lagrangian transformation matrix is defined as:

$$J = \frac{\partial x_i}{\partial X_j} \qquad (6)$$

Linear momentum, Eq.(3), is multiplied by the matrix J to produce the following:

5

$$\frac{D}{Dt}\left(u_i\frac{\partial x_i}{\partial X_j}\right) = \frac{\partial}{\partial X_j}\left(\frac{u_iu_i}{2} - gy\right) - \frac{1}{\rho}\frac{\partial p}{\partial X_j} \tag{7}$$

2.1. Homogeneous Fluid

For a homogeneous medium Eq.(1) is identically satisfied and Eq.(7) can be integrated as follows

$$\int \frac{D}{Dt}\left(u_i\frac{\partial x_i}{\partial X_j}\right) dt = \int \frac{\partial}{\partial X_j}\left(\frac{u_iu_i}{2} - gy - \frac{p}{\rho}\right) dt \tag{8}$$

such that

$$u_i\frac{\partial x_i}{\partial X_j} - a_j = \frac{\partial}{\partial X_j}\int\left(\frac{u_iu_i}{2} - gy - \frac{p}{\rho}\right) dt \tag{9}$$

where a_j is a constant of integration dependant on the material coordinates (X, Y). From Trusdell (1954) and Serrin (1959) one can define the Weber transformation

$$\frac{D\phi}{Dt} = \frac{u_iu_i}{2} - gy - \frac{p}{\rho} \tag{10}$$

such that Eq.(9) can then be written

$$u_i\frac{\partial x_i}{\partial X_j} = A_j + \frac{\partial \phi}{\partial X_j} \tag{11}$$

where A_j is a constant of integration and now:

$$\frac{DA_j}{Dt} = 0 \tag{12}$$

Eq.(11) can now be multiplied by the inverse of matrix J to produce the Clebsch decomposition:

$$u_i = A_j \frac{\partial X_j}{\partial x_i} + \frac{\partial \phi}{\partial x_i} \tag{13}$$

The rotational velocity field at $t = t_0$ is defined as

$$u_i^{r0} = \left(u_i - \frac{\partial \phi}{\partial x_i} \right) \Bigg|_{t = t_0} \tag{14}$$

and if one sets $X_i = x_i$ at $t = t_0$, then $u_j^{r0} = A_j$, and Eqs.(12) and (13) become

$$\frac{Du_j^{r0}}{Dt} = 0 \tag{15}$$

and

$$u_i = u_j^{r0} \frac{\partial X_j}{\partial x_i} + \frac{\partial \phi}{\partial x_i} \tag{16}$$

where u^{r0} is an upstream-generated shear that has been convected into the domain. Provided the initial condition $X_i = x_i$ is specified at $t = t_0$, a homogeneous, inviscid, incompressible flow can now be described by the scalar convection equations, Eqs.(5) and (15); continuity, Eq.(2); and the Clebsch decomposition, Eq.(16). From the Clebsch decomposition, Eq.(16), vorticity is defined as

$$\omega_i = \varepsilon_{ijk} \frac{\partial}{\partial x_j} \left(u_l^{r0} \frac{\partial X_l}{\partial x_k} \right) \tag{17}$$

7

where ε_{ijk} is the standard permutation tensor. From Eq.(17) it becomes clear that vorticity exits only within the presence of the redistributed shear that was generated upstream.

2.2. Stratified Fluid

For a stratified medium Eq.(7) is integrated

$$\int \frac{D}{Dt} \left(u_i \frac{\partial x_i}{\partial X_j} \right) dt = \int \frac{\partial}{\partial X_j} \left(\frac{u_i u_i}{2} - gy \right) dt - \int \frac{1}{\rho} \frac{\partial p}{\partial X_j} \, dt \qquad (18)$$

such that

$$u_i \frac{\partial x_i}{\partial X_j} - a_j = \frac{\partial}{\partial X_j} \int \left(\frac{u_i u_i}{2} - gy \right) dt - \frac{1}{\rho} \frac{\partial}{\partial X_j} \int p \, dt \qquad (19)$$

where, as in the homogeneous case, a_j is a constant of integration dependant on the material coordinates (X, Y). One can again define Weber transformations

$$\frac{D\phi}{Dt} = \frac{u_i u_i}{2} - gy \qquad (20)$$

$$\frac{D\psi}{Dt} = -p \qquad (21)$$

such that Eq.(19) can be written

$$u_i \frac{\partial x_i}{\partial X_j} = A_j + \frac{\partial \phi}{\partial X_j} + \frac{1}{\rho} \frac{\partial \psi}{\partial X_j} \qquad (22)$$

where A_j is a constant of integration that satisfies Eq.(12). The inverse of matrix J multiplies Eq.(22) to produce the Clebsch decomposition:

8

$$u_i = A_j \frac{\partial X_j}{\partial x_i} + \frac{\partial \phi}{\partial x_i} + \frac{1}{\rho} \frac{\partial \psi}{\partial x_i} \qquad (23)$$

A component of the rotational velocity field at $t = t_0$ can be defined as

$$u_i^{r0} = \left(u_i - \frac{\partial \phi}{\partial x_i} - \frac{1}{\rho} \frac{\partial \psi}{\partial x_i} \right) \Bigg|_{t = t_0} \qquad (24)$$

and if one sets $X_i = x_i$ at $t = t_0$, then $u_j^{r0} = A_j$ and Eq.(23) becomes

$$u_i = u_j^{r0} \frac{\partial X_j}{\partial x_i} + \frac{\partial \phi}{\partial x_i} + \frac{1}{\rho} \frac{\partial \psi}{\partial x_i} \qquad (25)$$

where u^{r0} is again an upstream-generated shear that has been convected into the domain. Provided the initial condition $X_i = x_i$ is specified at $t = t_0$, a stratified, inviscid, incompressible flow is now be described by the scalar convection equations, Eqs.(1), (5), (15), and (20); continuity, Eq.(2); and the Clebsch decomposition, Eq.(25). From the Clebsch decomposition, Eq.(25), vorticity is defined as

$$\omega_i = \varepsilon_{ijk} \frac{\partial}{\partial x_j} \left(u_l^{r0} \frac{\partial X_l}{\partial x_k} + \frac{1}{\rho} \frac{\partial \psi}{\partial x_k} \right) \qquad (26)$$

which implies that vorticity can exist in the presence of the upstream-generated shear or can be created by the presence of the density stratification. Furthermore, as the density field is redistributed throughout the flow, so too is the opportunity to generate vorticity.

3. UNSTEADY CONVECTION SCHEME

Convection equations (1), (5), (15), and (20) can be written as the decoupled scalar system:

$$\frac{\partial W}{\partial t} + \frac{\partial F}{\partial x} + \frac{\partial G}{\partial y} = H \tag{27}$$

This equation is solved by a cell-centered finite volume scheme that constructs a piecewise linear distribution over each of the finite volumes; characteristically convects information to an intermediate time level; and updates the cell-centered variables with a midpoint rule time integration.

To insure the production of a nonoscillatory solution, at least directionally, the piecewise linear distribution is constructed in a nonoscillatory manner. To avoid excessive amounts of damping, this distribution must be at least uniformly second order accurate. A one-dimensional interpolation can be written

$$W = W_i + S_i^x(x - x_i) \tag{28}$$

where S_i^x is the slope over each finite volume. The slope associated with Harten and Osher's (1987) uniformly second order accurate UNO2 scheme is written

$$S_i^x = \frac{Median(0, W_{i+1/2}^c - W_i, W_i - W_{i-1/2}^c)}{\Delta x/2} \tag{29}$$

where $W_{i+1/2}^c$ is obtained from a nonoscillatory quadratic interpolation

$$W_{i+1/2}^c = 0.5(W_i + W_{i+1}) - 0.25D_{i+1/2} \tag{30}$$

where

$$D_{i+1/2} = minmod(W_{i+1} - 2W_i + W_{i-1}, W_{i+2} - 2W_{i+1} + W_i) \tag{31}$$

and

$$minmod(a,b) = sign(a) \max(0, sign(ab) \min(|a|, |b|)) \tag{32}$$

Surface data is evaluated at time level $n + 1/2$ by following characteristics back to their spatial locations at time level n. For positive convection speeds, the surface data at time level $n + 1/2$ is written:

$$W_{i+1/2,j}^{n+1/2} = W_{i,j}^n + S_{i,j}^x \frac{\Delta x}{2}\left(1 - \frac{u_{i+1/2,j}\Delta t}{\Delta x}\right) - S_{i,j}^y \frac{v_{i+1/2,j}\Delta t}{2} \tag{33}$$

Once the surface data and their fluxes are constructed at the time level $n + 1/2$, the cell-centered values are updated by the midpoint rule

$$W_{i,j}^{n+1} = W_{i,j}^n - \Delta t\left(\frac{F_{i+1/2,j}^{n+1/2} - F_{i-1/2,j}^{n+1/2}}{\Delta x} + \frac{G_{i,j+1/2}^{n+1/2} - G_{i,j-1/2}^{n+1/2}}{\Delta y}\right) \tag{34}$$

where $F = Wu$ and $G = Wv$.

4. STEADY STATE POTENTIAL SCHEME

For a homogenous flow the continuity equation

$$\nabla \cdot \vec{v} = \frac{\partial}{\partial x_i}\left(u_j^{r0}\frac{\partial X_j}{\partial x_i} + \frac{\partial \phi}{\partial x_i}\right) = 0 \tag{35}$$

must be satisfied at each time step to produce the velocity potential ϕ. This equation is solved by the approximately LU factored scheme

$$[1 - \mu\alpha(\delta_x^+ + \delta_y^+)] \cdot [1 + \mu\alpha(\delta_x^- + \delta_y^-)]\Delta\phi_{ij} = \alpha\omega(\delta_x u + \delta_y v)_{ij} \tag{36}$$

where $\Delta\phi_{ij} = \tilde{\phi}_{ij} - \phi_{ij}$; μ and α are scalar constants of $o(1)$; ω is a relaxation parameter; and δ^+, δ^-, and δ are forward, backward, and central difference operators. For a stratified flow the continuity equation

$$\nabla \cdot \vec{v} = \frac{\partial}{\partial x_i} \left(u_j^{r0} \frac{\partial X_j}{\partial x_i} + \frac{\partial \phi}{\partial x_i} + \frac{1}{\rho} \frac{\partial \psi}{\partial x_i} \right) = 0 \tag{37}$$

must be satisfied at each time step to produce the velocity potential ψ. This equation is solved by the approximately LU factored scheme

$$\left[1 - \frac{\mu\alpha}{\rho} (\delta_x^+ + \delta_y^+) \right] \cdot \left[1 + \frac{\mu\alpha}{\rho} (\delta_x^- + \delta_y^-) \right] \Delta\psi_{ij} = \alpha\omega(\delta_x u + \delta_y v)_{ij} \tag{38}$$

where $\Delta\psi_{ij} = \tilde{\psi}_{ij} - \psi_{ij}$. The residuals, Eq.(35) and (37), are approximated by a finite volume formulation that constructs fluxes on the faces of each mesh cell. The scalar systems are then solved by two explicit sweeps through the domain, similar to the procedures developed by Anderson, Thomas, and Whitfield, (1986) and Yokota and Caughey (1988) for two factored, implicit time-marching schemes. The approximate LU scheme is also written within the framework of the multigrid method to accelerate these calculations to a steady state.

5. ANALYTICAL STEADY SHEAR FLOW

From Ho and Huerre (1984), a steady, quasi-two dimensional shear layer can be modelled

$$u = \bar{u} (1 + R \tanh \beta) \tag{39}$$

$$v = 0 \tag{40}$$

where $\beta = 0.5(y - y_c)/\theta$; $\bar{u} = 0.5(u_1 + u_2)$; $\Delta u = u_2 - u_1$; $R = 0.5\Delta u/\bar{u}$; θ is the momentum thickness; y_c is the centerline; and u_1 and u_2 are the velocities of the two coflowing streams.

5.1. Homogeneous Fluid

A Clebsch decomposition that satisfies Eqs.(2), (5), (15), (16), (39), and (40) can be written as

$$u'^0 = \bar{u}\,(1 + R \tanh \beta) - u_1 \tag{41}$$

$$v'^0 = 0 \tag{42}$$

$$X = x - \bar{u}t\,(1 + R \tanh \beta) \tag{43}$$

$$Y = y \tag{44}$$

$$\phi = u_1 x + \frac{\bar{u}Rt}{2} \tanh \beta\,(\Delta u + \bar{u}R \tanh \beta) \tag{45}$$

5.2. Stratified Fluid

For an immiscible, stratified media defined as

$$\rho = \rho_1 + (\rho_2 - \rho_1)\,H(y) \tag{46}$$

where $H(y)$ is the heaviside unit step function and ρ_1 and ρ_2 are the densities of the two fluids, a Clebsch decomposition that satisfies Eqs.(1), (2), (5), (15), (19), (25), (39), (40), and (46) can be written

$$u'^0 = \bar{u}\,(1 + R \tanh \beta) - u_1 \tag{47}$$

$$v'^0 = 0 \tag{48}$$

$$X = x - \bar{u}t\,(1 + R \tanh \beta) \tag{49}$$

$$Y = y \tag{50}$$

$$\psi = \rho gyt \tag{51}$$

$$\phi = u_1 x + \bar{u}t\,(1 + R \tanh \beta) \cdot \left(\frac{\dot{\bar{u}}}{2}\,(1 + R \tanh \beta) - u_1 \right) - gyt \tag{52}$$

6. NUMERICAL ASPECTS

Shear layer calculations, characterized by $u_1 = 4.0m/s$; $u_2 = 8.0m/s$; $\rho_1 = 1.0kg/m^3$; $\rho_2 = 0.9kg/m^3$; and $\theta = 2.0mm$, are performed on a 192x96 grid (Fig.1). This grid has a uniform streamwise spacing of $1.6mm$ and is algebraically stretched in the cross-stream direction. The cross-stream distribution has approximately 30 cells within the initial shear layer, 10 of which are within the momentum thickness θ. The smallest cell is $0.2mm$ thick and located at the centerline, while the computational domain is approximately $0.1m$ wide and $0.3m$ long.

The initial conditions are constructed analytically at $t = 0$ and the velocity potential ϕ is recast as a perturbation on a uniform flow. Thus

$$\phi = u_1 x + \tilde{\phi} \tag{53}$$

where $\tilde{\phi}$ is obtained from the continuity equation which is solved at each time step by an approximately factored LU scheme. The LU scheme is written within the framework of the multigrid method to accelerate these calculations to a steady state. At each time step, a six multigrid level W cycle converges the average residual to $0(10^{-14})$ within five iterations (Yokota 1992).

6.1. Homogeneous Fluid

An inviscid noflux or parallel flow condition

$$\frac{\partial u'^0}{\partial y} = \frac{\partial \tilde{\phi}}{\partial y} + u'^0 \frac{\partial X}{\partial y} = 0 \tag{54}$$

is specified at both the top and bottom boundaries of the domain, while the outflow condition

$$\frac{\partial^2 u'^0}{\partial x^2} = \frac{\partial^2 X}{\partial x^2} = \frac{\partial^2 \tilde{\phi}}{\partial y^2} + \frac{\partial}{\partial y}\left(u'^0 \frac{\partial X}{\partial y} \right) = \tilde{\phi}(x_l, y_b) = 0 \tag{55}$$

14

is specified at $x = x_l$. A steady inflow condition

$$u^{r0} = \bar{u}\,(1 + R \tanh \beta) - \mu_1$$

$$v^{r0} = \frac{\partial \tilde{\phi}}{\partial x} = 0 \qquad (56)$$

$$\frac{\partial X}{\partial x} = 1$$

can be specified at $x = x_0$ or modified accordingly for an unsteady simulation.

6.2. Stratified Fluid

The following inviscid noflux or parallel flow condition

$$\frac{\partial u^{r0}}{\partial y} = \frac{\partial \rho}{\partial y} = \frac{\partial \tilde{\phi}}{\partial y} + u^{r0}\frac{\partial X}{\partial y} + \frac{1}{\rho}\frac{\partial \psi}{\partial y} = 0 \qquad (57)$$

is specified at both the top and bottom boundaries of the domain, while the outflow condition

$$\frac{\partial^2 u^{r0}}{\partial x^2} = \frac{\partial^2 X}{\partial x^2} = \frac{\partial^2 \rho}{\partial x^2} = \frac{\partial^2 \tilde{\phi}}{\partial x^2} = \frac{\partial^2 \tilde{\phi}}{\partial y^2} + \frac{\partial}{\partial y}\left(u^{r0}\frac{\partial X}{\partial y} + \frac{1}{\rho}\frac{\partial \psi}{\partial y}\right) = 0 \qquad (58)$$

$$\psi(x_l, y_b) = \rho g y_b t$$

is specified at $x = x_l$. A steady inflow condition

$$u^{r0} = \bar{u}\,(1 + R \tanh \beta) - u_1$$

$$v^{r0} = \frac{\partial \tilde{\phi}}{\partial x} = \frac{\partial \psi}{\partial x} = 0 \qquad (59)$$

$$\frac{\partial X}{\partial x} = 1$$

and Eq.(46) are specified at $x = x_0$ and are again modified accordingly for an unsteady calculation.

The analytic steady shear flows, Eqs.41-45 for a homogeneous flow and Eqs.46-52 for a stratified flow, have been reproduced numerically to verify the fidelity of this Clebsch/Weber

15

decomposition approach. Both flows were reproduced accurately and a detailed investigation of the homogeneous simulation was performed with respect to the conservation of circulation and enstrophy (Yokota 1991). In both of these simulations, the absence of physical viscosity manifests itself at the centerline of the shear layer by admitting an infinite stretching and shearing of the X material lines. At the centerline of the shear layer, $\partial X/\partial y \to \infty$ as $t \to \infty$. In fact, it is this inviscid behavior that limits the overall accuracy of long duration or time-periodic calculations. On a fixed grid, the inability to resolve the infinite shearing of the X material lines to a given accuracy level makes the one-dimensional conditions

$$v = \frac{\partial \phi}{\partial y} + u^{r0} \frac{\partial X}{\partial y} = 0 \tag{60}$$

for a homogeneous flow and

$$v = \frac{\partial \phi}{\partial y} + u^{r0} \frac{\partial X}{\partial y} + \frac{1}{\rho} \frac{\partial \psi}{\partial y} = 0 \tag{61}$$

for a stratified flow increasingly difficult to satisfy at the centerline of the shear layer. These equations become numerically indeterminant as $t \to \infty$. Thus the development of an invisid shear instability is more likely to be caused by an unbounded, numerical centerline disturbance, rather than by the growth of a more physically consistent initial disturbance.

7. CENTERLINE FORCING OF A STEADY SHEAR LAYER

To simulate the vortical rollup of a two-dimensional shear layer, without the uncertainty of its numerical origin, the inflow boundary conditions, Eqs.(56) and (59), are modified with an oscillating centerline:

$$\beta = \frac{(y - \tilde{y}_c)}{2\theta} \tag{62}$$

16

$$\tilde{y}_c = y_c + K\theta \sin(\tilde{\omega}t) \tag{63}$$

$$\tilde{\omega} = \frac{2\pi S_n \bar{u}}{\theta} \tag{64}$$

where $S_n = 0.032$ is the Strouhal number of the shear layer's natural frequency (Ho and Heurre 1984) and K is a scalar constant. The chosen amplitude of this centerline oscillation is one tenth the momentum thickness ($K = 0.1$) and therefore confined to within the width of the smallest mesh cell. The shear layer's natural frequency, $96\,hz$, was chosen for this oscillation, while a constant time step size of $0.01\,ms$ (or $9.6x10^{-4}T$ where T is the period of the centerline oscillation) was used in the time advancement.

The initial conditions are assumed to exist for $-\infty < x > +\infty$ but in Fig.2 are shown only within the domain encompassed by the computational grid. The initial conditions for the u^{r0} and X material fields are identical for both the homogenous and stratified fluids, while the density interface of the stratified flow coincides with the centerline of the shear layer. If these simulations were to remain steady, the u^{r0} material lines and the density interface would remain identical to the initial conditions, while the X material field would shear continuously with the flow. For a steady flow, both the $\tilde{\phi}$ and ψ potential fields are initially zero and would evolve into the quasi-two-dimensional fields described by Eqs.51 and 52. However, in the following simulation an oscillating centerline disturbance renders the flow both two-dimensional and unsteady.

Within both the homogeneous and stratified fuids, an initial rollup of the shear layer results from an inviscid instability (Brown and Roshko 1974 and Saffman 1981). Given that the Froude number of these simulations is $F_r = \bar{u}/(g\theta)^{1/2} \simeq 60$, inertial effects will dominate those due to gravity and any gravitationally-induced upstream influence should be minimal. The vortical rollups produced within this stratified flow are not suppressed by gravity and are qualitatively similar to those found within its homogeneous counterpart.

For the stratified flow, the evolution of the u^{r0} and X material lines are shown in Figs.3 and 4. The evolution of the u^{r0} material lines, which are equivalent to unsteady streaklines

passing through the inflow boundary, reveals the initial development of the small amplitude waves, Fig.3a-c, their subsequent steepening, Fig.3d-e, and eventual rollup, Fig.3f-h. The evolution of the density interface is comparable but not equivalent to that of the u'^0 material lines since the inflow location of the density stratification remains constant while the centerline of the shear oscillates. During the development of this unsteady shear layer, the density interface undulates and steepens to produce a significant interfolding of the two fluids.

The inviscid shearing of the X material field, Fig.4, produces a temporally growing cross-stream gradient that can roll up when disturbed. Within this simulation, the shear flow instability develops from small amplitude wave to nonlinear rollup. As the X material field convects downstream, it both stretches and folds around the large vortical structures present within the flow.

The stretching and shearing of the redistributed shear layer can be seen within the evolution of the streamwise and cross-stream gradients of the X material field. Within the evolution of the streamwise gradient field, one can see the linear disturbances, Fig.5a-b, separate into a series of alternating regions of high and low streamwise stretching, Fig.5h. The inflow disturbances evolve into a number of spatially growing structures whose locations coincide with the steepening of the u'^0 material lines. Since the minimum streamwise gradient is always larger than the specified inflow boundary condition, no streamwise contraction of the X material field is produced within this flow.

The transition from small amplitude wave to nonlinear rollup is distinguishable within both the U'^0 material field and the streamwise gradient field, while its presence is much more subtle within the cross-stream gradient field. The centerline of the shear layer, located at the maximum cross-stream gradient, bends, breaks, and ultimately evolves into a number of discrete structures (Fig.6c). After the initial breakage, this gradient field is drawn, pinched, and redistributed into discrete clumps (Figs.6h). These structures, formed initially at the period of the inflow forcing, are continually stretched and shaped as they are convected with the flow. Fur-

thermore, because the inflow shear dominates the evolution of this flow, the X material field experiences no positive streamwise shearing.

From the evolving ψ potential field, Fig.7, one can see that disturbances are predominantly local to the vortical structures and parallel to the density stratification. Since vorticity is generated only by the gradients of ψ which are perpendicular to the density stratification, the evolution of this flow is again dominated more by the redistributed inflow shear than by the presence of the density stratification. Furthermore, little vorticity is generated inside the nonlinear rollups since the ψ potential field is relatively constant within their cores.

The time histories of circulation and enstrophy over the fixed computational domain are global indicators of the flow's unsteadiness. When the fluid is homogeneous and the flow is two-dimensional, both circulation and enstrophy will remain constant over a non-material domain only while the flow remains steady. The same is true for a stratified fluid only while the flow is both steady and one-dimensional.

The time histories of both the stratified and homogeneous simulations are plotted with respect to a nondimensional time which has been normalized by the period of the inflow forcing. While variations do exist, both the circulation and enstrophy histories of these two flow simulations are qualitatively similar. The density stratification does not significantly influence the evolution of the redistributed inflow shear. The oscillating circulation histories, Fig.8, are caused by a cross-stream velocity component that is being generated by the inflow forcing. The slight differences between these circulation histories can be attributed to the oscillating location of the inflow shear relative to the fixed density stratification.

The enstrophy histories, Fig.9, reflect the initial development of the small amplitude waves that transition into nonlinear structures after approximately two to three periods of the inflow forcing. Since the enstrophy histories are virtually identical, the disturbances that are responsible for the variations in the circulation histories have, at best, only a minor effect on the evolution of the redistributed inflow shear.

19

The primary vortical structures observed within this flow are similar, if not identical, to those seen within a homogenous flow (Yokota 1992). The qualitative behavior of these flows is due to the redistributed inflow shear; and while comparisons of the evolving material fields do not reveal any significant visual discrepancies, subtle differences do exist. Within these simulations, however, it is difficult to separate the evolution of the convected shear from that generated by the density stratification. While vorticity is being generated by the density stratification, its effect is weak, localized, and dominated by the redistributed inflow shear. A number of starting shear layers will be simulated in the following section to better investigate the behavior of a shear generated by a density stratification. These simulations will allow one to visually separate the redistributed shear from the shear generated by the density stratification.

8. CONVECTION AND PROPAGATION OF A STARTING INFLOW SHEAR

An inflow shear distribution is imposed upon an initially uniform flow to simulate the evolution of both a homogeneous and stratified starting shear layer. As this inflow shear is convected downstream, a vortex is generated at its leading edge. In the simulations to follow, the inflow shear is imposed abruptly upon the uniform flow, $\nabla \phi = u_1$. Thus the inflow is instantaneously accelerated to the one-dimensional shear distribution described by Eqs.39 and 40. Since the Froude number of these flows is $Fr = 60$, the evolution of the leading edge vortex will be dominated by inertial effects, unsuppressed by gravity, and similar within both fluids. Furthermore, because the inflow density stratification is identical to that of the initial flow, no buoyancy-driven disturbances are explicitly introduced from the inflow boundary.

These calculations are started with an initial X material field and density interface identical to those specified within the previous simulations. The initial u'^0 material field is assumed not to exit at $t = 0$ and a constant time step size of $0.01ms$ (or $9.6x10^{-4}T$ where T is the period of shear layer's natural frequency), is again used throughout these simulations.

After 1500 time steps, the homogeneous fluid's u'^0 and X material fields are shown in Fig.10, while these material fields, together with the density interface, are found in Fig.11 for the

stratified fluid. The u'^0 material fields, Figs.10a and 11a, are constructed from fluid particles tagged with the inflow shear and reveal both its advancing front and the location of its leading edge vortex. The leading edge vortex evolves in a qualitatively similar manner within both the homogeneous and stratified fluids.

The most significant difference between these two simulations is the presence of a downstream shear found within the stratified fluid. Downstream of the leading edge vortex and along the density stratification, the presence of this shear can be seen within the X material field, Fig.11b. Furthermore, the shear's quasi-two-dimensional appearance suggests that its propagation was rapid, one-dimensional, and independant of the leading edge vortex. The starting shear produces an inflow disturbance that generates vorticity as it propagates along the density interface. This vorticity is not convected from the inflow boundary. The circulation history, Fig.12, which is calculated over the fixed computational domain and normalized with respect to the shear layer's momentum thickness and natural frequency, gives this explanation further credence. While negative circulation grows linearly within both flows, an initial burst of vorticity is generated within the stratified fluid. Further evidence of this phenomenon can be obtained at a fixed downstream location by monitoring the streamwise velocity at two points equally spaced above and below the initial density interface. The difference between the velocities at points located at 55% of the domain's halfwidth above and below the density interface are monitored at a location 90% of the domain's length downstream from the inflow boundary. The time history of this difference is normalized by u_{ave}, shown in Fig.13, and reveals an abrupt creation of shear within the stratified fluid. While this shear is likely to change as the leading edge vortex eventually approaches and passes this downstream location, it is clear that a constant shear was generated downstream of the inflow boundary. This result is in contrast to the homogeneous fluid within which no downstream vorticity was created.

To gain an understanding, albeit limited, of how this downstream shear was generated, one can investigate the behavior of a one-dimensional velocity disturbance. Since we are prin-

cipally concerned with the behavior of the initial transient, a one-dimensional assumption is informative.

If upon a steady one-dimensional flow, $u = u_0$, one imposes a transient perturbation such that the resulting flow can be approximated as

$$u = u_0 + \varepsilon \tilde{u}_1 + \varepsilon^2 \tilde{u}_2 + \cdots \tag{65}$$

$$p = p_0 + \varepsilon p_1 + \varepsilon^2 p_2 + \cdots \tag{66}$$

$$\psi = \psi_0 + \varepsilon \psi_1 + \varepsilon^2 \psi_2 + \cdots \tag{67}$$

then after expanding this approximation within Eq.(3) and collecting all first order terms, one is left with the unsteady equation:

$$\frac{\partial \tilde{u}_1}{\partial t} = -\frac{1}{\rho} \frac{\partial p_1}{\partial x} \tag{68}$$

Since the flow was initially irrotational, $u'^0 = 0$ and therefore $\partial \psi_0 / \partial x = 0$. By expanding Eq.(21) and collecting first order terms, one is left with the unsteady equation:

$$\frac{\partial \psi_1}{\partial t} + u_0 \frac{\partial \psi_1}{\partial x} = -p_1 \tag{69}$$

If one defines the linearized material derivative

$$\frac{D^0}{Dt} = \frac{\partial}{\partial t} + u_0 \frac{\partial}{\partial x} \tag{70}$$

then:

$$\frac{D^0}{Dt} \left(\frac{\partial \psi_1}{\partial x} \right) = -\frac{\partial p_1}{\partial x} \tag{71}$$

Thus a velocity disturbance will generate a pressure gradient that will in turn induce a change in the gradient of ψ along the linearized streamwise direction. Furthermore a shear will be generated along the density stratification since

$$\omega = \frac{\partial}{\partial x}\left(\frac{1}{\rho}\frac{\partial \psi}{\partial y}\right) - \frac{\partial}{\partial y}\left(\frac{1}{\rho}\frac{\partial \psi}{\partial x}\right) \simeq -\frac{\partial}{\partial y}\left(\frac{1}{\rho}\right)\frac{\partial \psi}{\partial x} \tag{72}$$

and the density interface is unlikely to remain undisturbed. For a stably stratified flow, where $\rho_2 - \rho_1 < 0$, velocity transients can produce the following two behaviors.

I)

$$if \quad \frac{\partial \tilde{u}_1}{\partial t} > 0 \quad \Rightarrow \quad \frac{\partial p_1}{\partial x} < 0 \quad \Rightarrow \quad \frac{D^0}{Dt}\left(\frac{\partial \psi_1}{\partial x}\right) > 0$$

which implies that an acceleration will produce an increase in the linearized streamwise gradient of ψ_1 and ultimately the creation of negative vorticity. This scenario corresponds to the proceeding simulations where an inflow shear was imposed abruptly upon $\nabla \phi = u_1$. In those simulations the inflow was accelerated to the shear described by Eqs.39 and 40, and negative vorticity was created downstream of the leading edge vortex.

II)

$$if \quad \frac{\partial \tilde{u}_1}{\partial t} < 0 \quad \Rightarrow \quad \frac{\partial p_1}{\partial x} > 0 \quad \Rightarrow \quad \frac{D^0}{Dt}\left(\frac{\partial \psi_1}{\partial x}\right) < 0$$

which implies that a deceleration will produce a decrease in the linearized streamwise gradient of ψ_1 and the generation of positive vorticity. This behavior is verified in the following simu-

lation where the inflow of the initially uniform flow, $\nabla\phi = u_2$, is instantaneously decelerated to the shear distribution described by Eqs.39 and 40.

The initial u'^0 and X material fields, density interface, and time step size, are identical to those specified within the previous simulations. The u'^0 and X material fields, as well as the density interface, can be seen after 1500 time steps in Fig.14. The u'^0 material field is constructed from fluid particles tagged with the decelerated inflow shear distribution and identifies both the location of the advancing front and its leading edge vortex. Again the presence of the leading edge vortex can be seen within the X material field; however, unlike the previous simulation, the downstream-generated shear is positive in magnitude.

For completeness, a third simulation is performed for an initially uniform flow of $\nabla\phi = u_{ave}$. Here the upper stream is instantaneously accelerated to u_2 while the lower stream is simultaneously decelerated to u_1. The integrated change in the inflow velocity is zero and consequently a downstream shear should not be generated. The u'^0 and X material fields, and the density interface, are shown after 1500 time steps in Fig.15. The u'^0 material field, which is constructed from fluid particles tagged with both the accelerated and decelerated inflow shear distribution, identifies both the location of the advancing front and its leading edge vortex. The development of the leading edge vortex is again similar to that found within the previous simulations, however, there is no evidence of a downstream-generated shear. The evidence of vorticity, a telltale shearing of the X material field, is not found in Fig.15b. It is also important to note that this behavior is independant of the stratification's placement, relative to the centerline of the inflow shear. Simulations in which the location of the density stratification did not coincide with the centerline of the inflow shear also evolved without creating a downstream shear.

The circulation histories of the three stratified flow simulations are shown in Fig.16. From these comparisons one can readily identify the shear that was generated when $\nabla\phi = u_1$ and $\nabla\phi = u_2$. This behavior is also seen within the downstream velocity differences generated within these simulations, Fig.17. One can see that an equal but opposite downstream shear was gen-

erated when $\nabla\phi = u_1$ and $\nabla\phi = u_2$. Furthermore, this shear is related to the change in velocity and not to a change in momentum.

The leading edge vortex within each of these simulations displaces the density interface at similar downstream locations; however, the vertical depth of these displacements is most shallow when $\nabla\phi = u_1$ and increases in depth from $\nabla\phi = u_{ave}$ to $\nabla\phi = u_2$. This behavior is consistent with the increasing absolute inflow momentum change associated with these three simulations.

These simulations support the belief that an integrated change in the inflow velocity is responsible for generating the downstream shear. Buoyancy or momentum do not directly control the creation of this shear. Moreover, when gravity was explicitly set to zero, similar results were produced, further suggesting that buoyancy is not the mechanism by which this downstream shear is generated.

Laminar horizontal jets in linearly stratifed fluids with Froude numbers of $Fr < 1$ have been investigated analytically by List (1971), numerically by Peyret (1976), and experimentally by Voropayev, Afanasyev, and Filippov (1991). Upstream effects are usually of primary interest within flows having these Froude numbers; these investigations, as such, focused primarily upon the localized influence of the jet inflow itself. Since the density stratifications within these investigations were linear and flow visualizations were centered primarily around the inflow region, significant evidence of a downstream-generated shear was not observed. However, despite the linear stratification's more subtle influence, Peyret (1976) did observe some downstream effects:

The fluid injected at $x = 0$ pushes ahead of it the ambiant fluid, which remains, to some extent, channelled by the effect of the buoyancy force, which tends to prevent downward motion.......Hence the perturbations created by the penetration of the jet are felt at very large distances ahead of it.

While acknowledging the dominance of buoyancy effects within low Froude number flows, it is still possible that this downstream phenomena was triggered by the initial inflow velocity disturbance and not by the bulk movement of fluid induced by the continuously penetrating jet. The preceeding simulations support the belief that a downstream shear is generated by an inflow velocity disturbance and not by the presence of gravity. Furthermore, the downstream shears were generated quicker than can be attributed to, or hindered by, buoyancy effects.

In the absence of any redistributed inflow vorticity, the behavior of a shear generated by the presence of a density stratification will be investigated within the following section. A shear will be generated within an initially irrotational flow by a pulsed uniform inflow. Since this flow is free of any redistributed inflow shear, the resulting simulation should become time-periodic.

9. SHEAR GENERATED BY AN OSCILLATING IRROTATIONAL INFLOW

A third and final series of calculations simulates the generation of a shear by an oscillating irrotational inflow. Given the unsteady uniform flow

$$
\begin{aligned}
u &= u_\infty \left(1 + K \sin \tilde{\omega} t\right) \\
v &= 0
\end{aligned}
\tag{73}
$$

a Clebsch decomposition that satisfies Eqs.(1), (2), (5), (15), (19), (25), (46), and (73) can be written:

$$
u'^0 = 0
\tag{74}
$$

$$
v'^0 = 0
\tag{75}
$$

$$
X = x - u_\infty \left(t - \frac{K}{\omega} \cos \tilde{\omega} t\right)
\tag{76}
$$

$$
Y = y
\tag{77}
$$

$$\psi = \rho x u_\infty K \sin \tilde{\omega} t + \rho g y t \tag{78}$$

$$\phi = u_\infty x - g y t + \frac{u_\infty^2 t}{2} \left(\frac{k^2}{2} - 1 \right) - \frac{u_\infty^2 K^2}{8\tilde{\omega}} \sin 2\tilde{\omega} t \tag{79}$$

For the numerical simulation of this unsteady flow to remain one-dimensional, the following condition

$$v = -gt + \frac{1}{\rho} \frac{\partial \psi}{\partial y} = 0 \tag{80}$$

must be satisfied at each time step. This equation is identically satisfied if $g = 0$ or if ρ were constant. However, for a stratified fluid in a nonvanishing gravitational field, Eq.(80) is satisfied only when the density stratification, Eq.(46), is reproduced exactly. Since this stratification is discontinuous, it cannot be represented numerically without some diffusion and therefore disturbances are generated at this interface. The existence of gravity, coupled with an inability to reproduce a discontinuous density stratification, prevents this simulation from remaining one-dimensional. Thus, as in the case of the steady shear layer, the transition to an unsteady two-dimensional flow will be caused by a numerical limitation. However, one can avoid this numerical uncertainty by forcing the flow with an unsteady inflow condition.

The evolution of an unsteady, irrotational inflow, Eq.(73), is simulated by assuming the initial conditions

$$\begin{aligned} u'^0 &= v'^0 = \psi = \tilde{\phi} = 0 \\ X &= x \\ Y &= y \\ \phi &= u_\infty x + \tilde{\phi} \end{aligned} \tag{81}$$

are perturbed by the unsteady inflow condition

27

$$u'^0 = v'^0 = \frac{\partial \psi}{\partial x} = 0$$

$$\frac{\partial \tilde{\phi}}{\partial x} = u_\infty K \sin \tilde{\omega} t \tag{82}$$

where $u_\infty = 6 \, m/s$, $K = 0.5$ is a scalar constant, ρ is defined by Eq.(46), and $\tilde{\omega} = 100 \, hz$. From Eqs.(68)-(72) one recognizes that this unsteady inflow is capable of generating a downstream shear. However, unlike the previous simulations, this shear will not be quasi-two-dimensional, nor will it be independant of time. This simulation is the numerical counterpart to the classic wave-maker problem (Yih 1980, Wehausen 1991).

For the following simulation, the initial X material field and density stratification are identical to those specified in the previous calculations, and a constant time step size of 0.01 ms (or $1x10^{-3}T$ where T is the period of the inflow forcing) is again used throughout.

Since the imposed inflow is irrotational, an infinite shearing of the X material lines will not occur, and a time-periodic behavior can be reproduced numerically. A time-periodic flow is achieved after approximately 8 periods of the inflow forcing and is evident within the time histories of circulation and enstropy, Fig.18 and 19, respectively. Within these figures, circulation, enstropy, and time are nondimensionalized by the shear layer's natural frequency and momentum thickness. The circulation history is centered on a positive, nonzero mean, a behavior that is not unexpected since the unsteady one-dimensional flow, Eqs.(74-79), is irrotational only while the density interface remains undisturbed. This asymmetric behavior also exists within the enstrophy history which, along with circulation, takes the approximate form

$$\Gamma(t) = \int \omega(x,y,t) \, da \; \propto \; \sin \tilde{\omega} t + 0.2556 \tag{83}$$

$$E(t) = \int \omega^2(x,y,t)\, da \;\propto\; \left(\sin \tilde{\omega}t + 0.2556 \right)^2 \qquad (84)$$

where $\Gamma(t)$, $E(t)$, and $\omega(x,y,t)$ are the time dependent functions of circulation, enstrophy, and vorticity. These results imply that

$$E(t) \;\propto\; \Gamma^2(t) \qquad (85)$$

which is satisfied by the separable representation:

$$\omega(x,y,t) \;\simeq\; \bar{\omega}(x,y)\left(\sin \tilde{\omega}t + 0.2556 \right) \qquad (86)$$

The behavior of this vorticity field is largely that of a spatial distribution, periodically growing and decaying in time.

The evolution of this time-periodic flow can be illustrated within a sequence of results over one period of the inflow forcing. The evolution of the inflow $\tilde{\phi}$ potential disturbances can be seen in Fig.20. These periodic disturbances are convected from the inflow boundary and distorted along the density interface. Each of these spatially growing disturbances grows and decays over one period of the inflow forcing.

The unsteadiness of this flow can also be seen within the seeming erratic behavior of the X material field, Fig.21. Along the density interface the X material field undergoes only minor amounts of local shearing, both positive and negative in sign. As these spatially growing regions convect with the flow, they undergo a fairly complicated temporal pattern of growth and decay. First, a shear is not simply generated at the inflow boundary and convected downstream. Both the mechanism by which this vorticity is generated and its downstream development continues to be controlled by the inflow velocity disturbances. Furthermore, it is clear that, relative to the forced shear layer, little fluid mixing occurs within this flow. No wrapping or folding of material lines occurs around vortical structures of any significant virulence. While vorticity is

periodically generated in the streamwise direction, its effect on the material field is clearly ephemeral.

This flow's overall structure is not immediately obvious within the X material field, which undergoes only minor amounts of localized shearing and stretching. Fortunately, the same is not true of its gradient fields. The streamwise gradient field, Fig.22, evolves into a series of doublet-like structures which contain regions of both high and low streamwise stretching. The minimum streamwise gradient is less than the specified inflow boundary condition and implies that this flow, unlike the forced shear layer simulation, undergoes both streamwise contraction and stretching.

The cross-stream gradient field, Fig.23, also reveals the presence of an alternating series of streamwise structures, positive and negative in magnitude. While these structures are convected from the inflow boundary, their individual strengths and sizes are continually fluctuating in response to the inflow forcing. The maximum cross-stream gradient remains constant while its minimum counterpart oscillates significantly. There is a clear duality to the structure of this flow.

The density interface, Fig.24, oscillates in a spatially growing manner that remains linear in structure and is symptomatic of poor fluid mixing. This displacement, while comparable in amplitude to what was produced by the forced shear layer, incurs very little interfolding of the two fluids. While this flow is both unsteady and vortical, the mixing of the two fluids is not very efficient.

To better appreciate the relatively complicated behavior of this flow, a sequence of results is used to illustrate the evolution of the unsteady vortical field. The temporal locations of these results, relative to one period in the circulation and enstrophy histories, are shown in Figs.26 and 27. During the time elapsed between Fig.25a-d, the flow is dominated by structures of diminishing negative vorticity. Moreover, the trace structures of positive vorticity disappear, and only begin to reappear as negative vorticity vanishes. Fig.25e-h shows how these newly emerging structures of positive vorticity grow, dominate the flow, diffuse, and eventually begin

to disappear. It is only as they begin to vanish that their negative counterparts begin to reappear. As before, the appearance of positive vorticity is preceded by a local minimum in the circulation history, while local maximums are followed by the appearance of negative vorticity. These transitions occur near concave down-to-concave up inflection points in the enstrophy history where the inflow is being either accelerated or decelerated towards the mean flow. From these results it is clear that while positive and negative vorticity grow and decay in a manner diametrically opposed to one another, at no point in time is this flow irrotational.

10. CONCLUDING REMARKS

A kinematic decomposition of the incompressible Euler equations can be used to separate a velocity field into rotational and irrotational components. The rotational component is constructed from a series of complex-lamellar fields while the irrotational component is evaluated from a scalar potential field. By decomposing the velocity field into rotational and irrotational components, one can identify the origins of various shear disturbances. By knowing the transport equations that govern these components, one can determine how these disturbances are convected or propagated throughout the flow.

This approach was used to investigate three different flows, each of which was rendered both two-dimensional and unsteady by an inflow velocity disturbance. The first simulation, the centerline forcing of a steady shear layer, was dominated by its redistributed inflow shear and not significantly influenced by its density stratification. The shear layer disturbances, which evolve from small amplitude waves to nonlinear rollups, are qualitatively similar within both a homogeneous and stratified fluid.

In the second series of calculations, a starting shear layer, significant differences between the homogeneous and stratified flows were found. Unique to the stratified fluid is the inflow velocity disturbance's ability to generate a downstream shear. Furthermore, this shear is created by the density stratification but is independant of gravity.

31

In the final simulation, an oscillating irrotational inflow was used to generate a stratified vortical flow. In the absence of any redistributed inflow vorticity, this simulation was singularly dependant upon the presence of the density stratification. A series of spatially growing vortical structures, both positive and negative in magnitude, were periodically created along the oscillating density interface. These structures were found to periodically grow and decay at the frequency of the inflow forcing and in a manner diametrically opposed to one another.

The strength of this kinematic approach lies in its ability to visualize fluid mixing quantitatively. In each of the preceding simulations, this aspect of the Clebsch/Weber decomposition was useful in investigating the flows more fully.

11. ACKNOWLEDGMENT

REFERENCES

Anderson, W.K., Thomas, J.L., and Whitfield, D.L., 1986 "Multigrid Acceleration of the Flux Split Euler Equations." *AIAA Paper 86-274*, AIAA 24th Aerospace Sciences Meeting, Reno, Nevada.

Atassi, H.M., and Scott, J.R., 1988 "Analysis of Nonuniform subsonic Flows About a Row of Moving Bodies." *Proceedings of the Fourth International Symposium on Unsteady Aerodynamics and Aeroelasticity of Turbomachines and Propellers.* Gallus, H.E., and Servaty, S., ed., pp. 39-67.

Brown, G.L., and Roshko, A., 1974 "On the density effects in turbulent mixing layers." *Journal of Fluid Mechanics,* no. 64, pp. 775-816.

Chang, S.-C., and Adamczyk, J.J., 1985a "A New Approach for Solving the Three-Dimensional Steady Euler Equations. I. General Theory." *Journal of Computational Physics,* vol. 60, pp. 23-40.

Chang, S.-C., and Adamczyk, J.J., 1985b "A New Approach for Solving the Three-Dimensional Steady Euler Equations. II. Application to Secondary Flows in a Turning Channel." *Journal of Computational Physics,* vol. 60, pp. 41-61.

Ecer, A., and Akay, H.U., 1983 "A Finite Element Formulation for Steady Transonic Euler Equations." *AIAA Journal,* vol. 21, no. 3, pp. 343-350.

Goldstein, M.E., 1978 "Unsteady vortical and entropic distortions of potential flows round arbitrary obstacles." *Journal of Fluid Mechanics*, no. 89, pp. 433-468.

Grossman, B., 1983 "The Computation of Inviscid Rotational Gasdynamic Flows using an Alternate Velocity Decomposition." *AIAA Paper 83-1900*, Proceedings of the AIAA 6th Computational Fluid Dynamics Conference, Danvers, Massachusetts.

Harten, A., and Osher, S., 1987 "Uniformly Higher-Order Accurate Nonoscillatory Schemes I.," *SIAM Journal of Numerical Analysis*, vol. 24, pp. 279-309.

Hawthorne, W.R., 1966 "On the Theory of Shear Flows." MIT Gas Turbine Laboratory Report no. 88.

Ho, C.-M., and Huerre, P., 1984 "Perturbed Free Shear Layers." *Annual Review of Fluid Dynamics*, vol. 16, pp. 365-424.

Hunt, J.C.R., 1987 "Vorticity and vortex dynamics in complex turbulent flows." *Trans. Can. Soc. Mech. Engrs.*, no. 11, pp. 21-35.

Hunt, J.C.R., and Hussain, F., 1991 "A note on velocity, vorticity, and helicity of inviscid fluid elements." *Journal of Fluid Mechanics*, no. 229, pp. 569-587.

Lacor, C., and Hirsch, Ch., 1982 "Rotational flow calculations in three-dimensional blade passages." *ASME Paper 82-GT-316*.

List, E.J., 1971 "Laminar momentum jets in a stratified fluid." *Journal of Fluid Mechanics*, no. 45, pp. 561-574.

Marris, A.W., 1964 "Generation of secondary vorticity in a stratified fluid." *Journal of Fluid Mechanics*, no. 20, pp. 177-181.

Murman, E.M., and Stremel, P.M., 1982 "A Vortex Wake Capturing Method for Potential Flow Calculation." *AIAA Paper 82-0947*.

Ottino, J.M., 1982 "Description of mixing with diffusion and reaction in terms of the concept of material surfaces." *Journal of Fluid Mechanics*, no. 114, pp. 83-103.

Peyret, R., 1976 "Unsteady evolution of a horizontal jet in a stratified fluid." *Journal of Fluid Mechanics*, no. 78, pp. 49-63.

Saffman, P.C., 1981 " Coherent Structures in Turbulent Flow." *The Role of Coherent Structures in Modelling Turbulence and Mixing*, Jimenez, J., ed., Lecture Notes in Physics, no. 136, pp. 1-9.

Serrin, J., 1959 "Mathematical Principles of Classical Fluid Mechanics." *Encyclopedia of Physics*, Flugge, S., ed., Springer Verlag, Berlin, vol. VIII/1, pp. 125 -263.

Steinhoff, J., and Suryanarayana, K., 1983 "The Treatment of Vortex Sheets in Compressible Potential Flow." *AIAA Paper 83-1881*, Proceedings of the AIAA 6th Computational Fluid Dynamics Conference, Danvers, Massachusetts.

Trusdell, C., 1954 *The Kinematics of Vorticity*. Indiana University Press, Bloomington, Indiana.

Voropayev, S.I., Afanasyev, Ya.D., and Filippov, I.A., 1991 "Horizontal jets and vortex dipoles in a stratified fluid." *Journal of Fluid Mechanics*, no. 227, pp. 543-566.

Wehausen, J.V., 1991 "Wave Maker in a Two-Layer Fluid." *Mathematical Approaches in Hydrodynamics,* Miloh, T., ed., SIAM, Philadelphia, pp. 163-172.

Yih, C.-S., 1960 "Exact solutions for steady two-dimensional flow of a stratified fluid." *Journal of Fluid Mechanics,* no. 9, pp. 161-174.

Yih, C.-S., 1980 *Stratified Flows.* Academic Press, New York, New York.

Yokota, J.W., and Caughey, D.A., 1988 "An LU Implicit Multigrid Algorithm for the Three-Dimensional Euler Equations." *AIAA Journal,* vol. 26, pp. 1061-1069.

Yokota, J.W., 1992 "Vorticity Dynamics of Inviscid Shear Layers." *AIAA Paper 92-0420,* AIAA 30th Aerospace Sciences Meeting, Reno, Nevada.
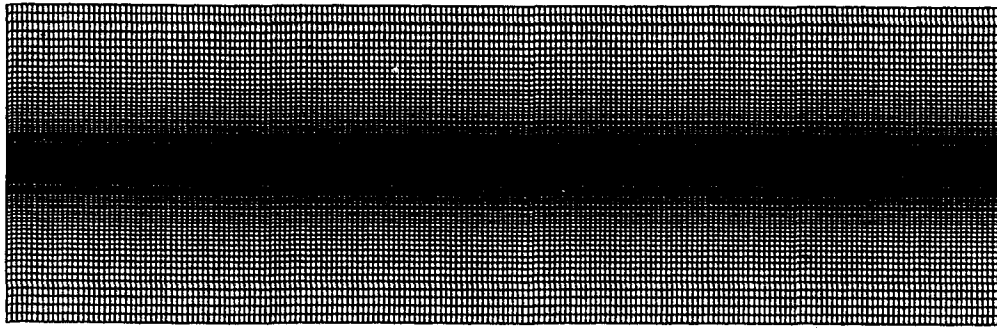
Figure 1.—Grid.
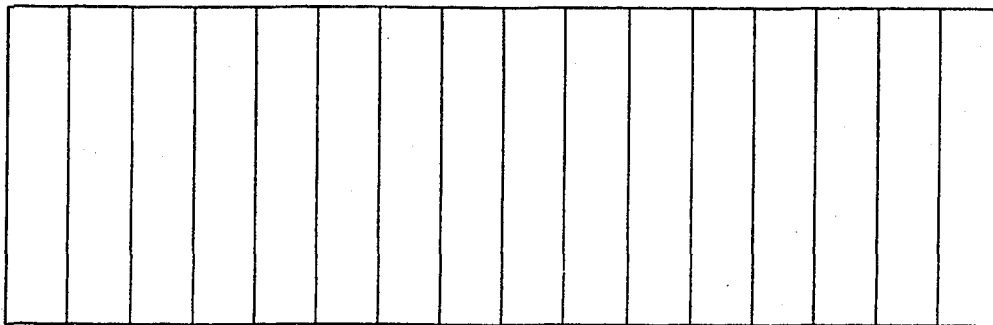
MIN= -0.9992   MAX=   -0.6904   INC=   0.0193
X CONTOURS

(a) X material field.
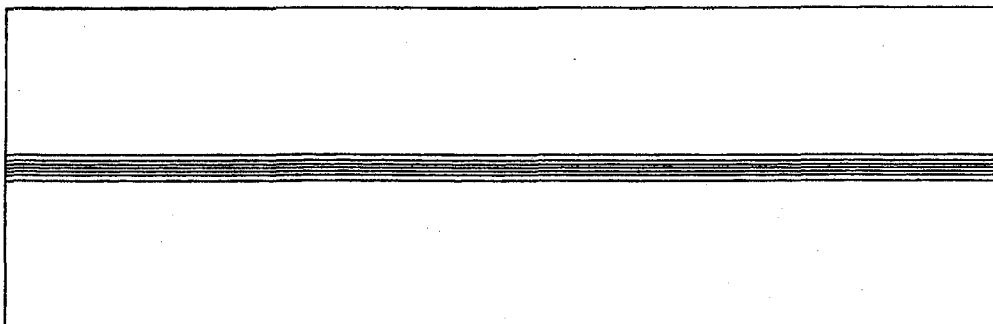
MIN=   0.5000   MAX=   3.5000   INC=   0.5000
URO CONTOURS

(b) u^{r0} material field.

Figure 2.—Initial conditions.
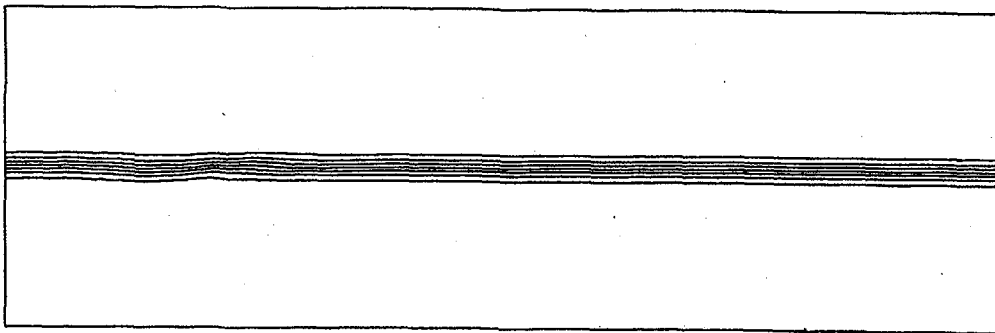
(a) t = 0.96.
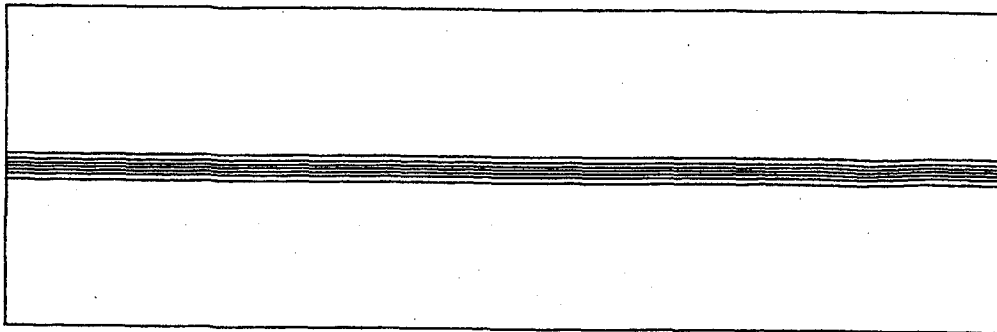
(b) t = 1.44.
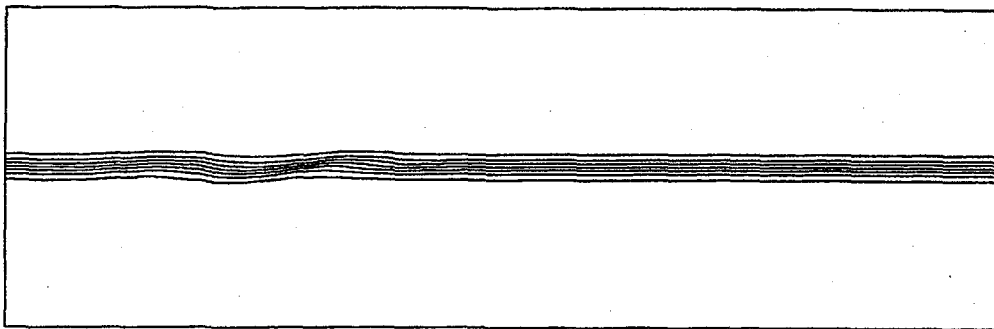
(c) t = 1.92.
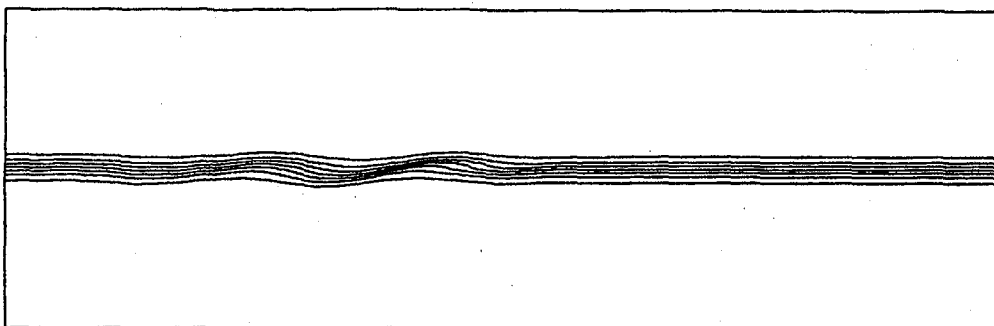
MIN=   0.5000   MAX=   3.5000   INC=   0.5000
URO CONTOURS

(d) t = 2.40.

Figure 3.—U^{r0} material field: forced stratified shear layer.
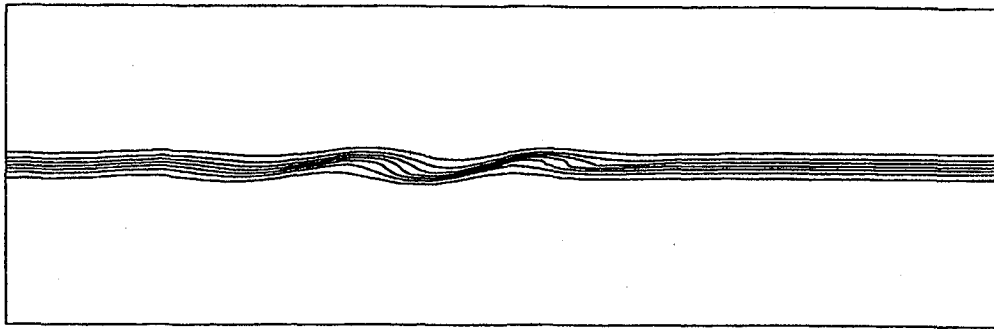
(e) t = 2.88.
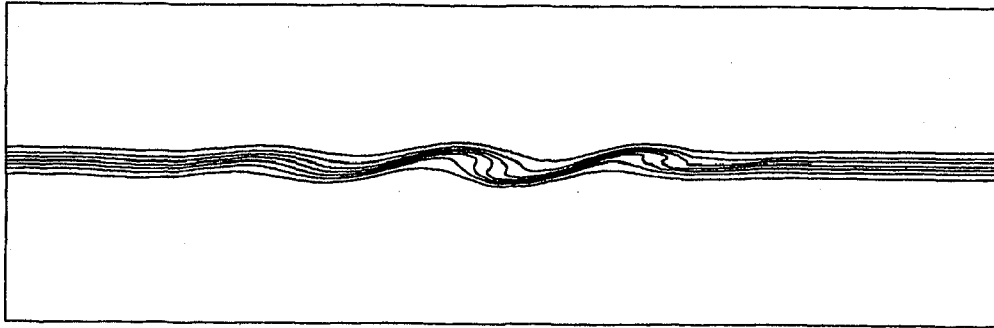
(f) t = 3.36.
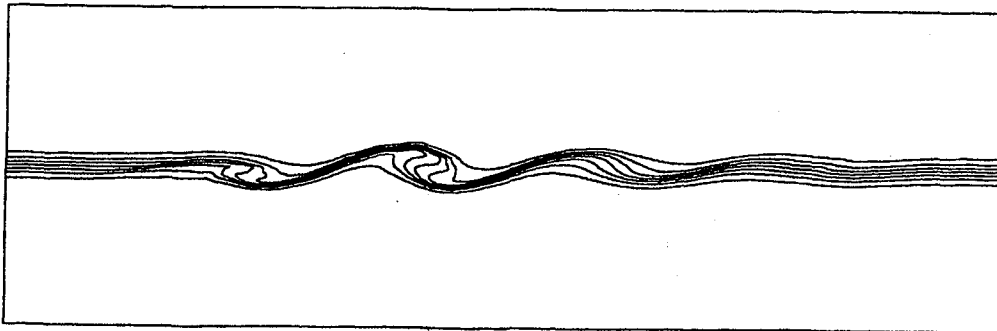
(g) t = 3.84.
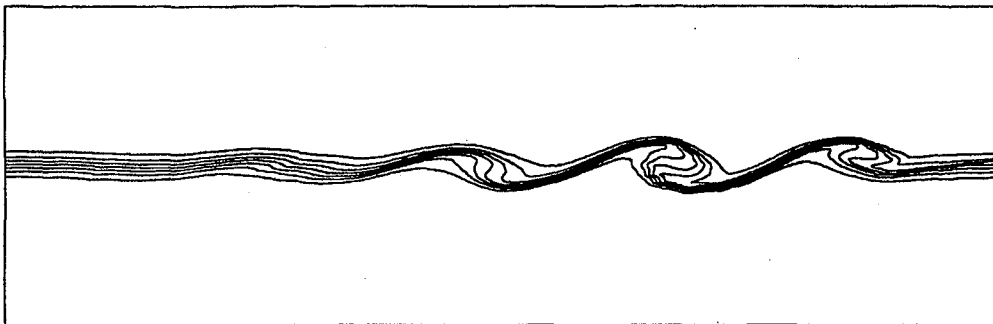
MIN=   0.5000   MAX=   3.5000   INC=   0.5000
URO CONTOURS

(h) t = 4.32.

Figure 3.—Concluded.
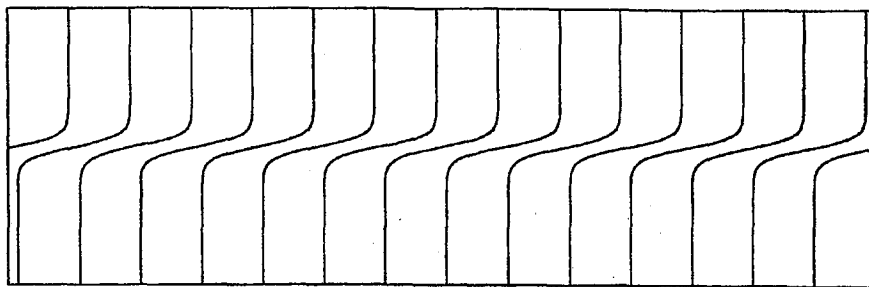
MIN= -1.0792   MAX=   -0.7304   INC=   0.0218
X CONTOURS

(a) t = 0.96.
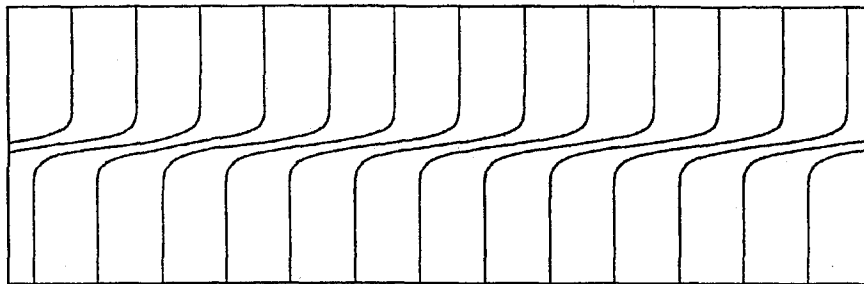
MIN= -1.1192   MAX=   -0.7504   INC=   0.0231
X CONTOURS

(b) t = 1.44.
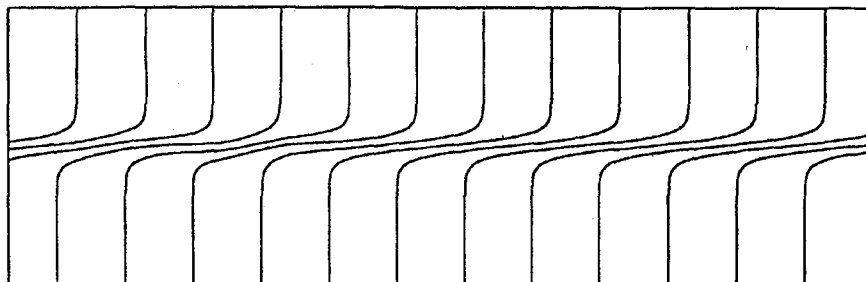
MIN= -1.1592   MAX=   -0.7704   INC=   0.0243
X CONTOURS

(c) t = 1.92.
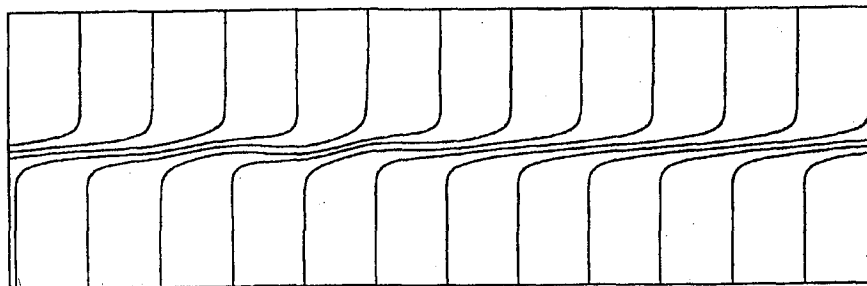
MIN= -1.1992   MAX=   -0.7904   INC=   0.0256
X CONTOURS

(d) t = 2.40.

Figure 4.—X material field: forced stratified shear layer.
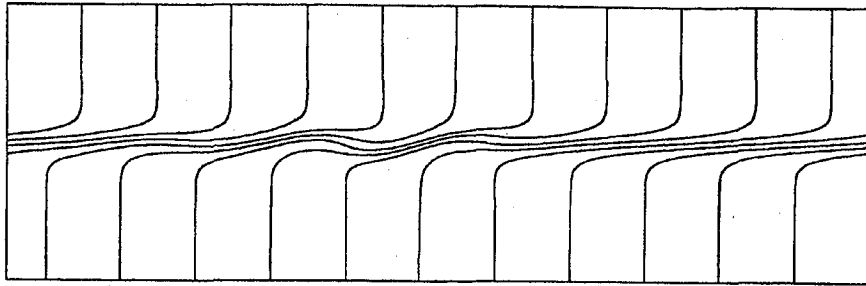
MIN= -1.2392   MAX=   -0.8104   INC=   0.0268
X CONTOURS

(e) t = 2.88.
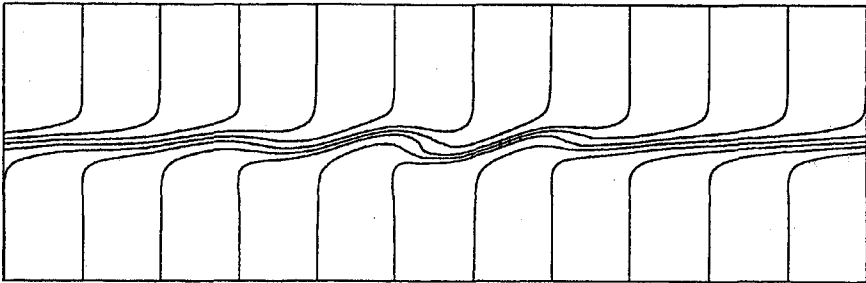
MIN= -1.2792   MAX=   -0.8304   INC=   0.0281
X CONTOURS

(f) t = 3.36.
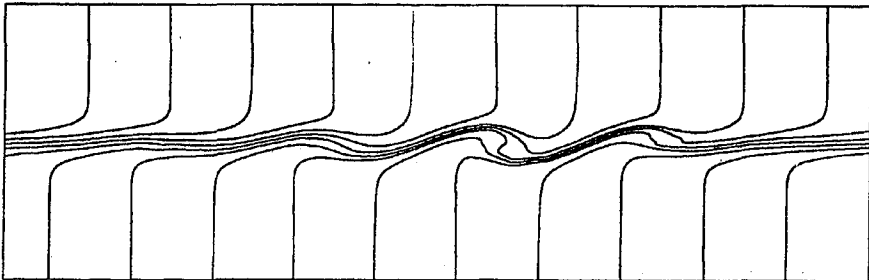
MIN= -1.3192   MAX=   -0.8504   INC=   0.0293
X CONTOURS

(g) t = 3.84.
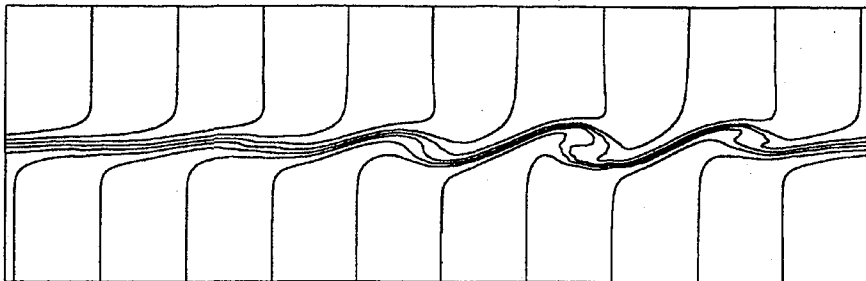
MIN= -1.3592   MAX=   -0.8704   INC=   0.0306
X CONTOURS

(h) t = 4.32.

Figure 4.—Concluded.
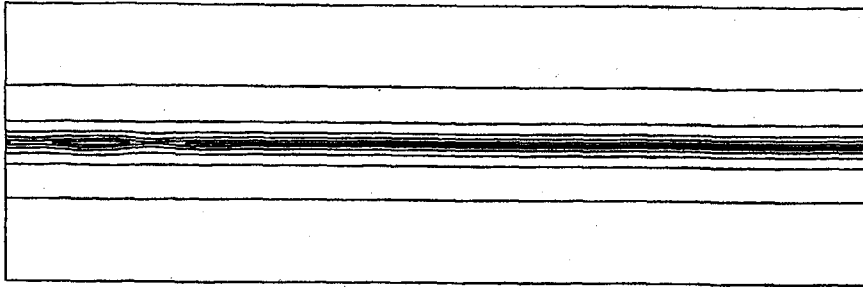
MIN = 0.125E 01   MAX = 0.794E 01   INC = 0.134E 01
STREAMWISE GRADIENT OF X

(a) t = 0.96.
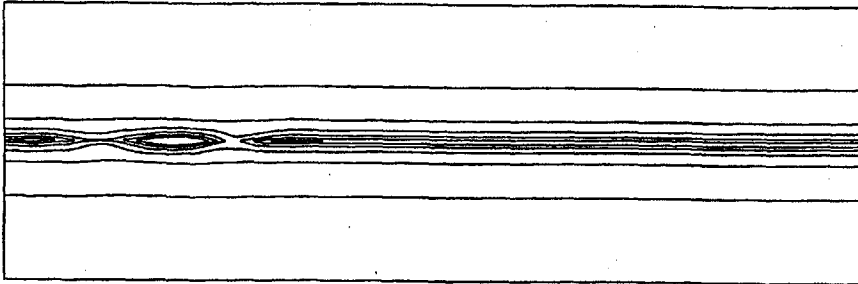
MIN = 0.125E 01   MAX = 0.809E 01   INC = 0.137E 01
STREAMWISE GRADIENT OF X

(b) t = 1.44.
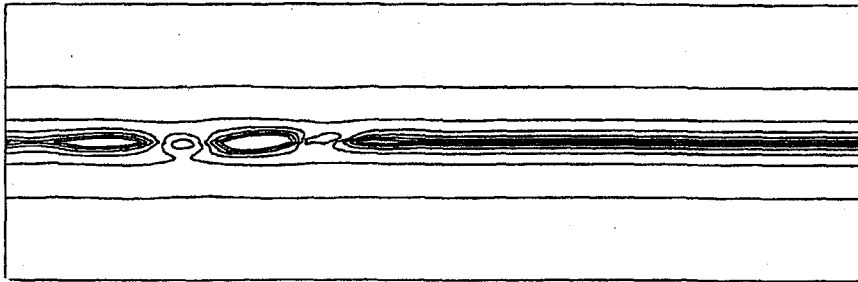
MIN = 0.125E 01   MAX = 0.786E 01   INC = 0.132E 01
STREAMWISE GRADIENT OF X

(c) t = 1.92.
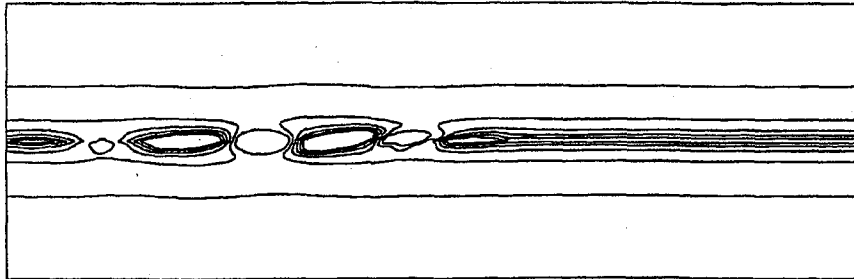
MIN = 0.125E 01   MAX = 0.816E 01   INC = 0.138E 01
STREAMWISE GRADIENT OF X

(d) t = 2.40.

Figure 5.—Streamwise gradient of the X material field: forced stratified shear layer.
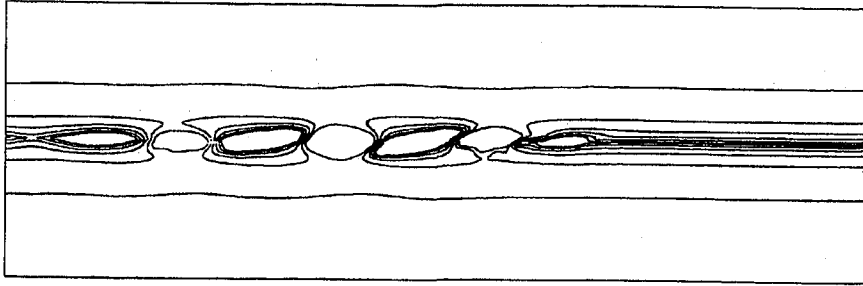
MIN = 0.125E 01   MAX = 0.779E 01   INC = 0.131E 01
STREAMWISE GRADIENT OF X

(e) t = 2.88.
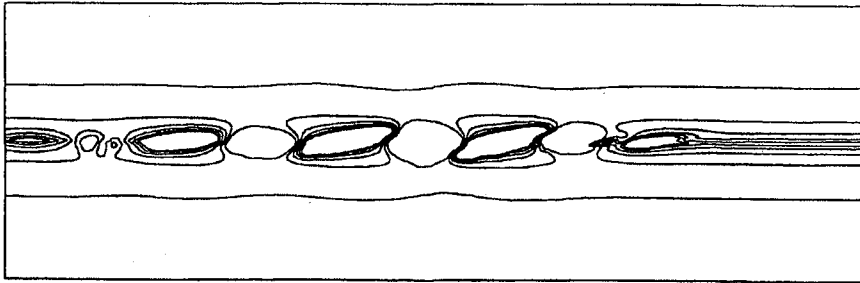
MIN = 0.125E 01   MAX = 0.823E 01   INC = 0.140E 01
STREAMWISE GRADIENT OF X

(f) t = 3.36.
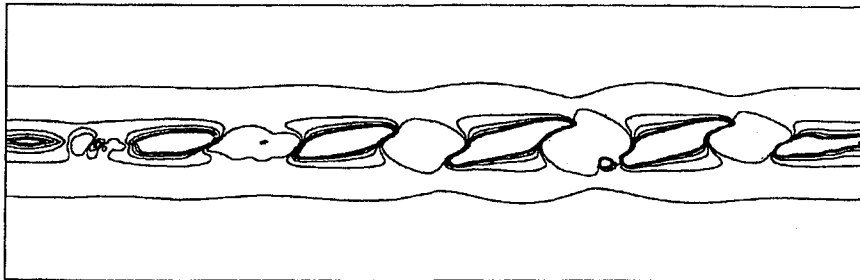
MIN = 0.125E 01   MAX = 0.774E 01   INC = 0.130E 01
STREAMWISE GRADIENT OF X

(g) t = 3.84.
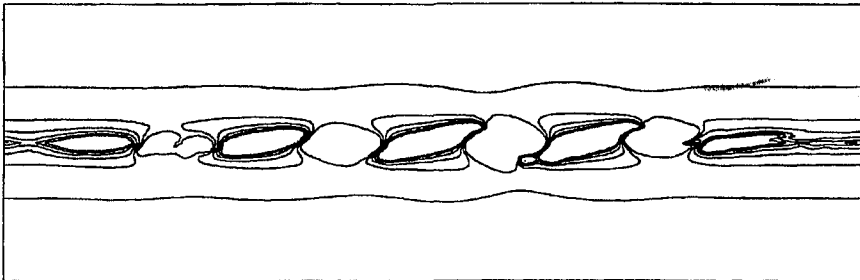
MIN = 0.125E 01   MAX = 0.828E 01   INC = 0.141E 01
STREAMWISE GRADIENT OF X

(h) t = 4.32.

Figure 5.—Concluded.

41
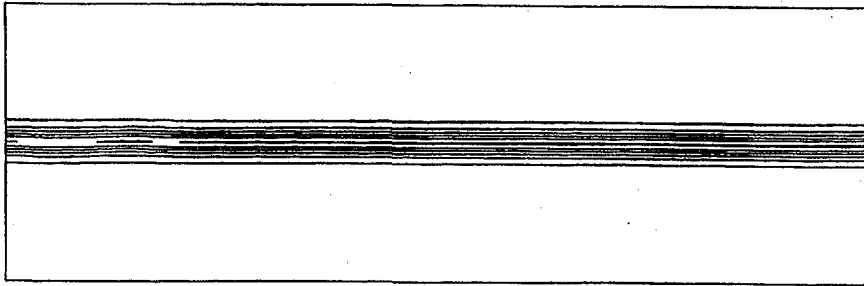
MIN = -0.505E 01   MAX =-0.500E 00   INC = 0.910E 00
CROSS-STREAM GRADIENT OF X

(a) t = 0.96.
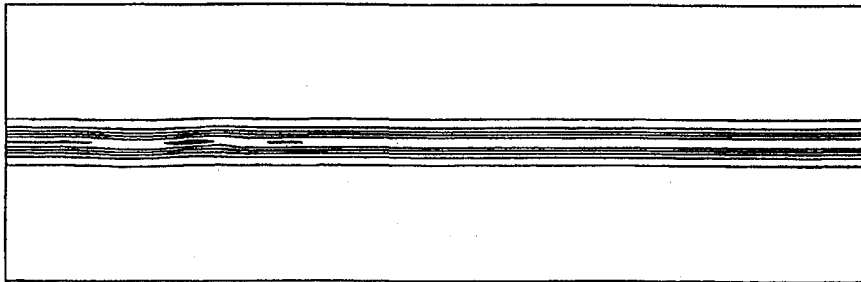
MIN = -0.764E 01   MAX =-0.500E 00   INC = 0.143E 01
CROSS-STREAM GRADIENT OF X

(b) t = 1.44.
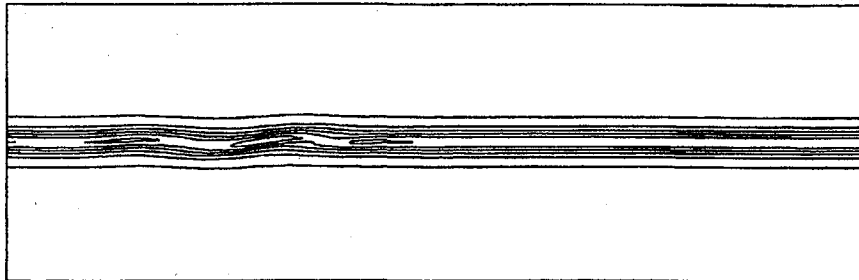
MIN = -0.102E 02   MAX =-0.500E 00   INC = 0.193E 01
CROSS-STREAM GRADIENT OF X

(c) t = 1.92.
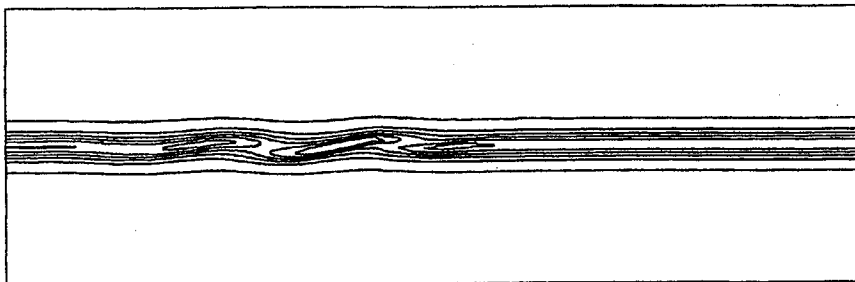
MIN = -0.128E 02   MAX =-0.500E 00   INC = 0.246E 01
CROSS-STREAM GRADIENT OF X

(d) t = 2.40.

Figure 6.—Cross-stream gradient of the X material field: forced stratified shear layer.
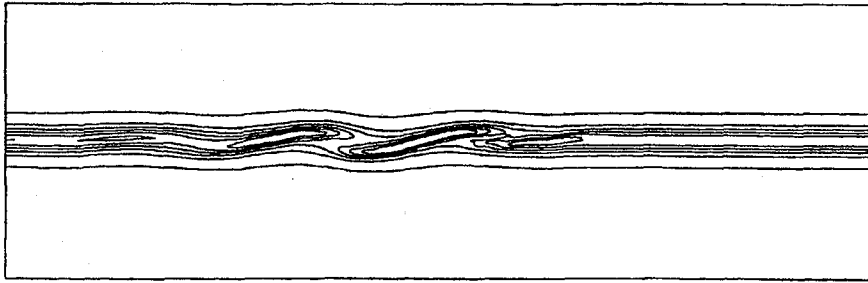
MIN = -0.153E 02   MAX =-0.500E 00   INC = 0.295E 01
CROSS-STREAM GRADIENT OF X

(e) t = 2.88.
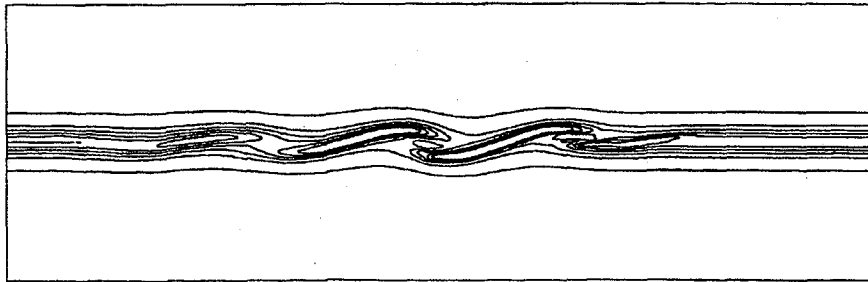
MIN = -0.179E 02   MAX =-0.500E 00   INC = 0.348E 01
CROSS-STREAM GRADIENT OF X

(f) t = 3.36.
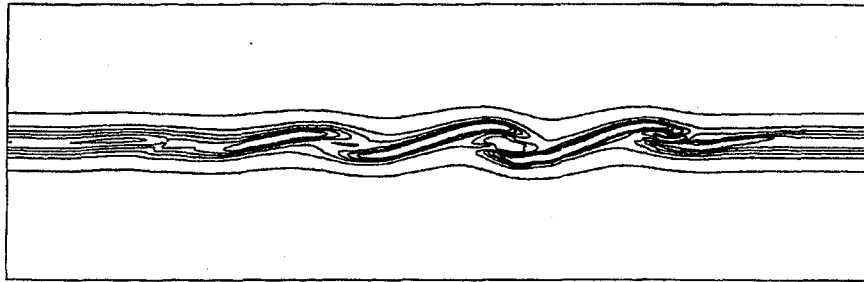
MIN = -0.204E 02   MAX =-0.500E 00   INC = 0.397E 01
CROSS-STREAM GRADIENT OF X

(g) t = 3.84.
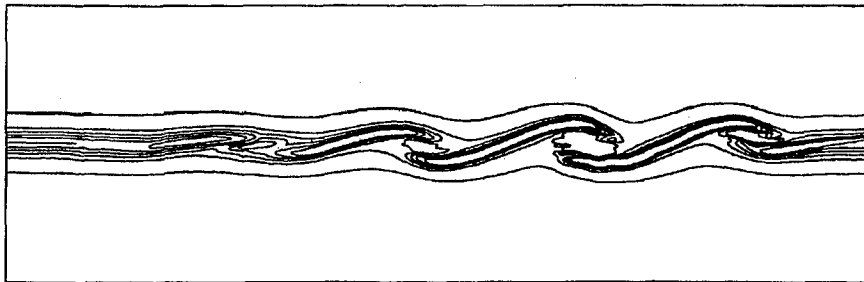
MIN = -0.230E 02   MAX =-0.500E 00   INC = 0.451E 01
CROSS-STREAM GRADIENT OF X

(h) t = 4.32.

Figure 6.—Concluded.
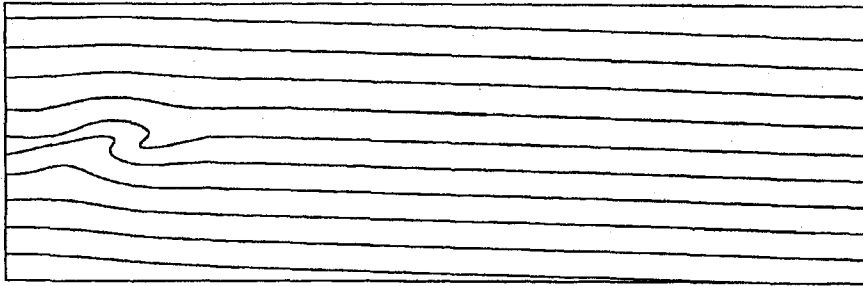
MIN = -0.576E-02   MAX = 0.370E-02   INC = 0.898E-03
PSI CONTOURS

(a) t = 0.96.
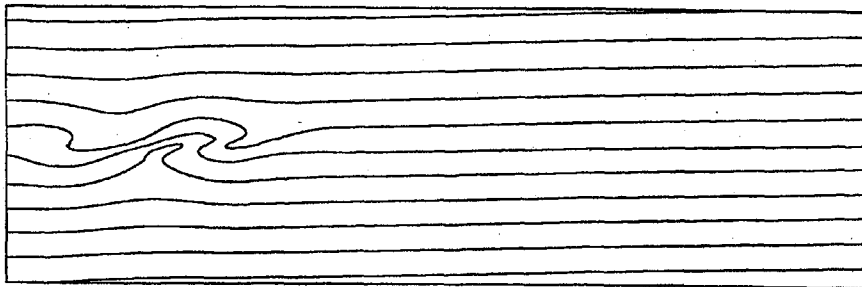
MIN = -0.617E-02   MAX = 0.733E-02   INC = 0.128E-02
PSI CONTOURS

(b) t = 1.44.
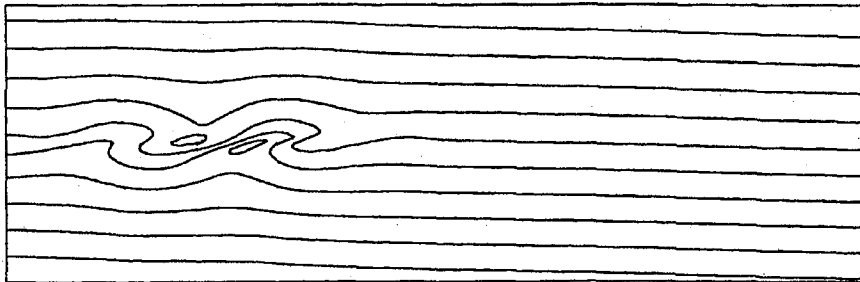
MIN = -0.111E-01   MAX = 0.752E-02   INC = 0.177E-02
PSI CONTOURS

(c) t = 1.92.
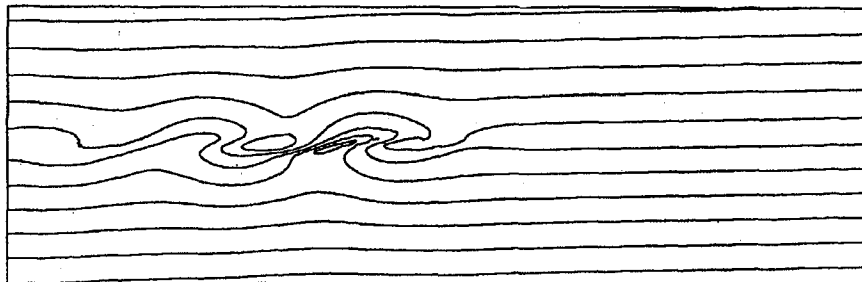
MIN = -0.104E-01   MAX = 0.120E-01   INC = 0.213E-02
PSI CONTOURS

(d) t = 2.40.

Figure 7.—Ψ potential field: forced stratified shear layer.

44
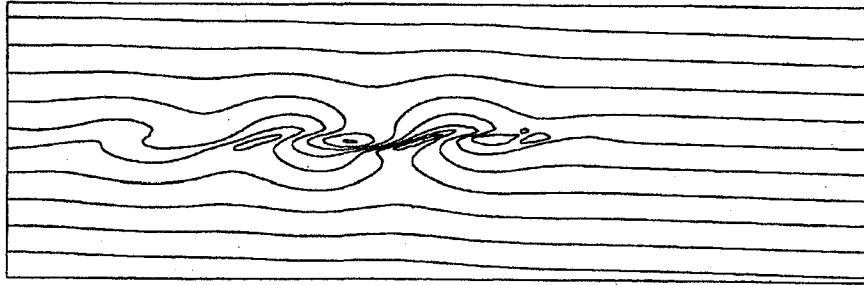
MIN = -0.164E-01   MAX = 0.113E-01   INC = 0.263E-02
PSI CONTOURS

(e) t = 2.88.
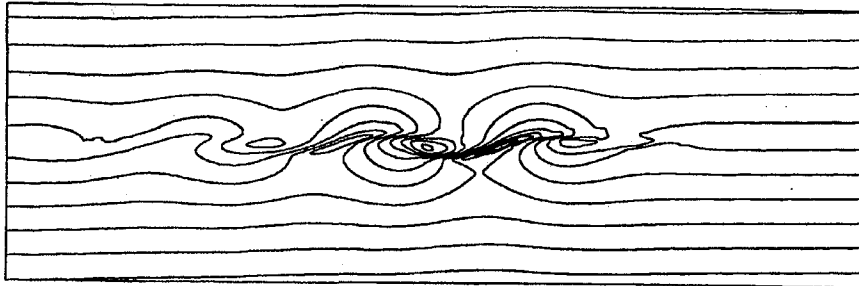
MIN = -0.149E-01   MAX = 0.165E-01   INC = 0.298E-02
PSI CONTOURS

·(f) t = 3.36.
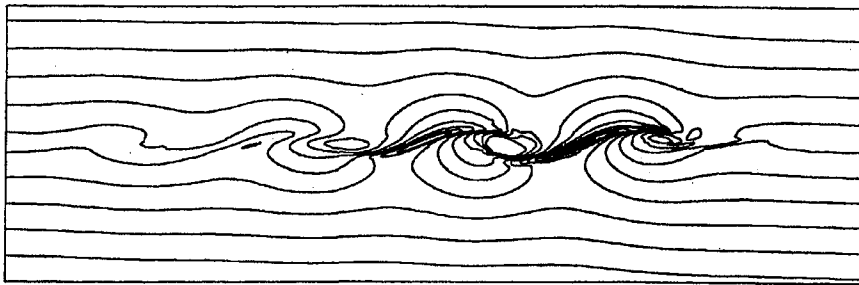
MIN = -0.219E-01   MAX = 0.148E-01   INC = 0.348E-02
PSI CONTOURS

(g) t = 3.84.
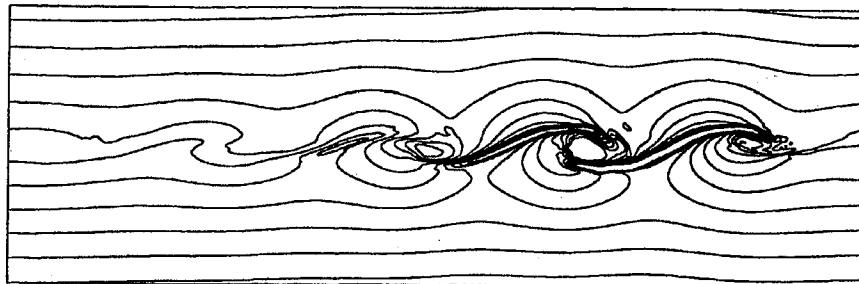
MIN = -0.201E-01   MAX = 0.202E-01   INC = 0.383E-02
PSI CONTOURS

(h) t = 4.32.

Figure 7.—Concluded.
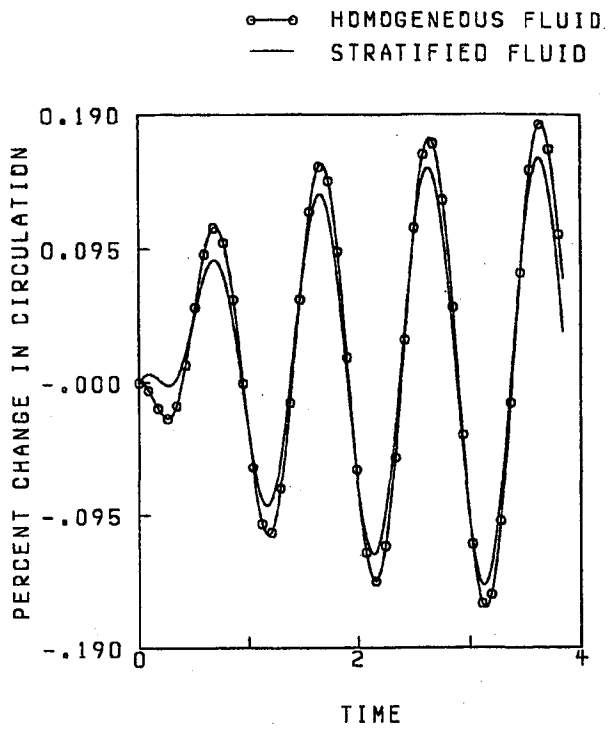
Figure 8.—Circulation history: forced shear layers.
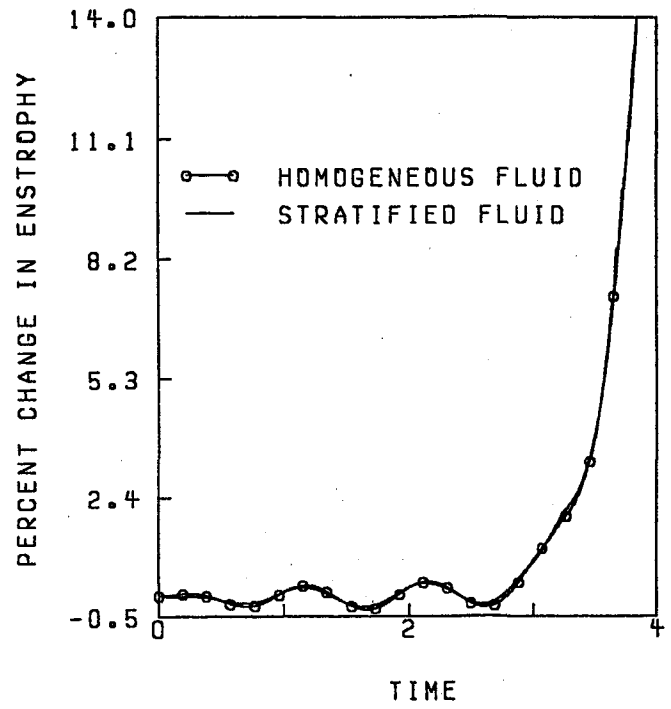
Figure 9.—Enstrophy history: forced shear layers.

MIN= 0.5000   MAX= 3.5000   INC= 0.5000
URO CONTOURS

(a) U^{r0} material field.

MIN= -1.1185   MAX= -0.7802   INC= 0.0211
X CONTOURS
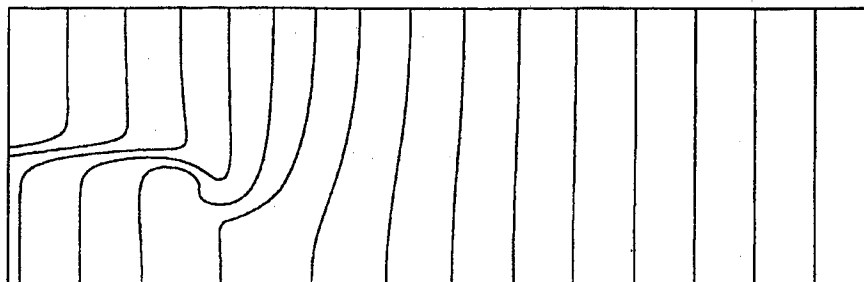
(b) X material field.

Figure 10.—Homogeneous starting shear layer - $\nabla_\phi = u_1$ at t = 1.44.

46

(a) U^{r0} material field.

(b) X material field.

(c) Density interface.

Figure 11.—Stratified starting shear layer - $\nabla_\phi = u_1$ at t = 1.44.

125.0

-187.5

CIRCULATION

-500.0

-812.5

-1125.0

○——○ HOMOGENEOUS FLUID
—— STRATIFIED FLUID

0.00   0.75   1.50

TIME
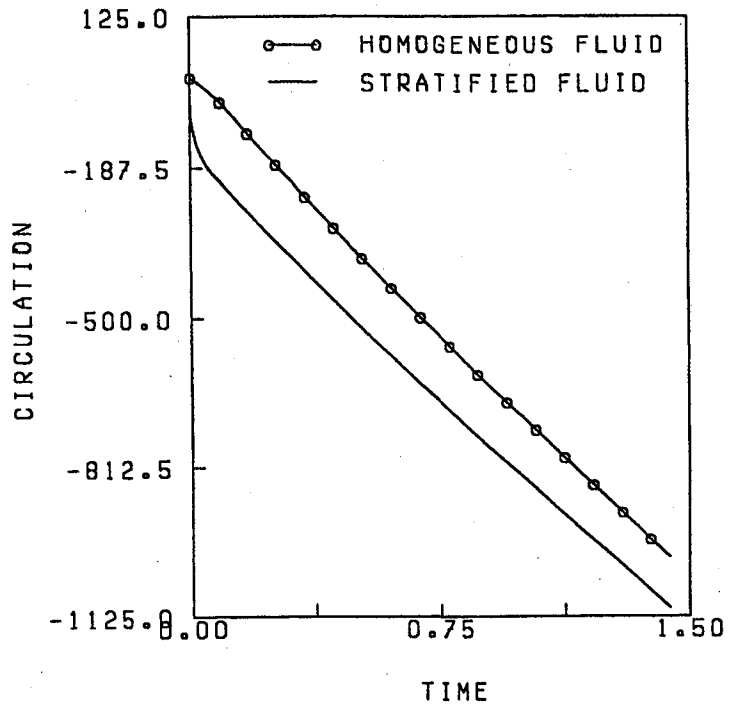
Figure 12.—Circulation history: starting shear layer - $\nabla_\phi = u_1$.

3.6

PERCENT DIFF. IN STREAMWISE VELOCITY

1.8

0.0

-1.8

-3.6

○——○ HOMOGENEOUS FLUID
—— STRATIFIED FLUID

0.00   0.75   1.50

TIME
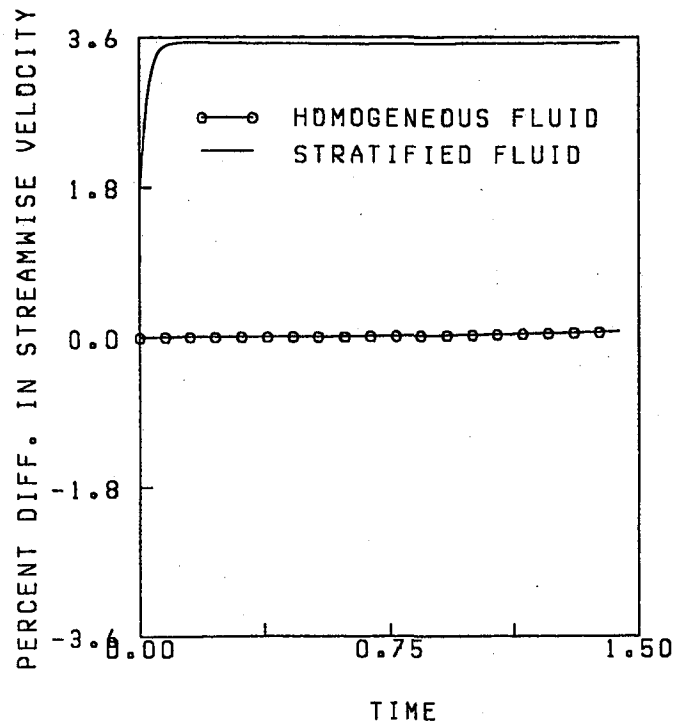
Figure 13.—Streamwise velocity difference: starting shear layer - $\nabla_\phi = u_1$.
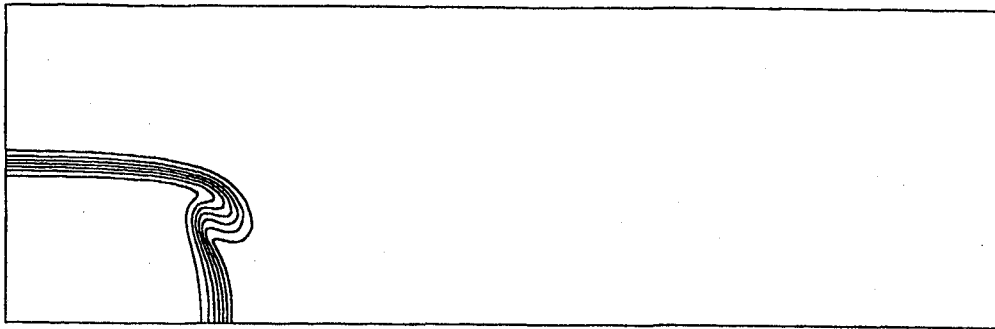
MIN= -3.5000   MAX= -0.5000   INC= 0.5000
URO CONTOURS

(a) U^{r0} material field.
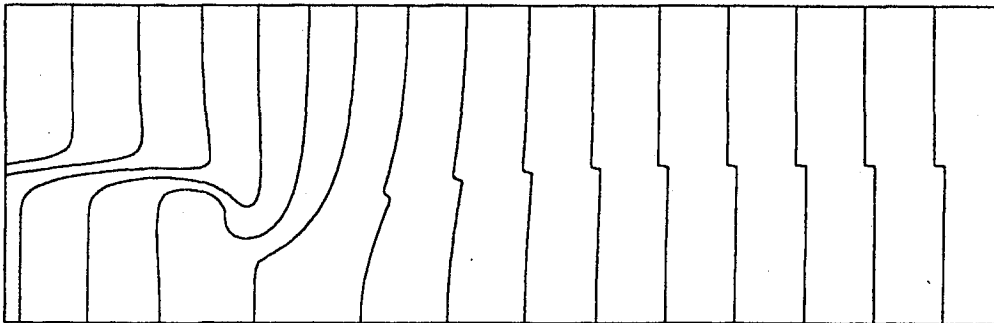
MIN= -1.1190   MAX= -0.7792   INC= 0.0212
X CONTOURS

(b) X material field.
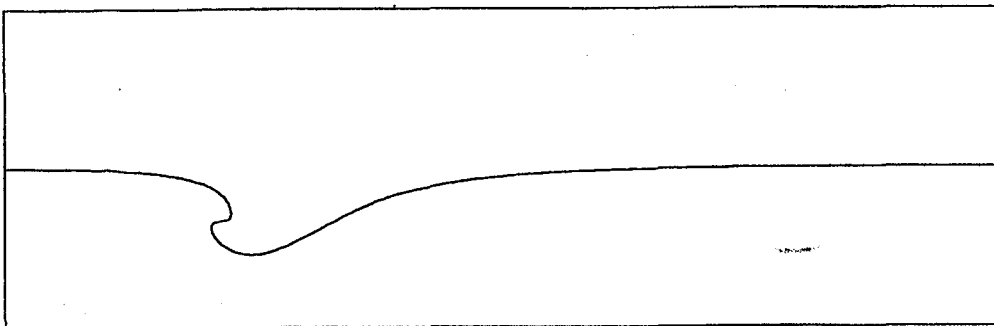
(c) Density interface.

Figure 14.—Stratified starting shear layer - $\nabla_\phi = u_2$ at t = 1.44.
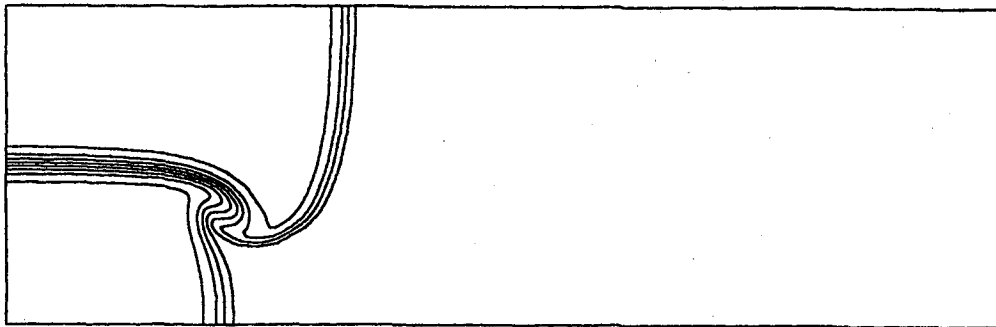
MIN= -1.7500   MAX=   1.7500   INC=   0.5000
URO CONTOURS

(a) U^{ro} material field.
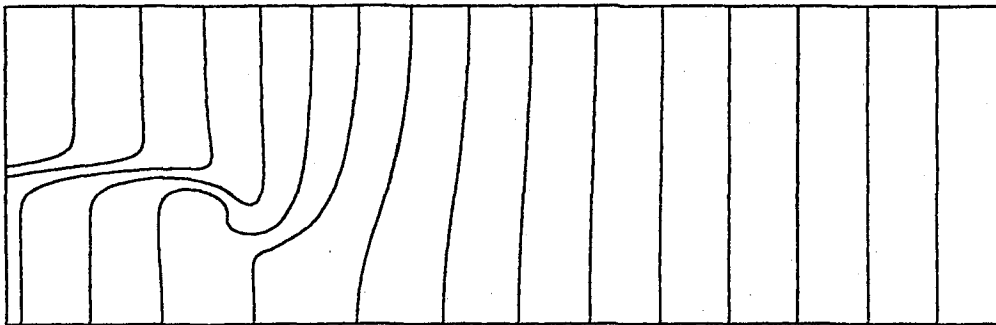
MIN= -1.1187   MAX=   -0.7805   INC=   0.0211
X CONTOURS

(b) X material field.
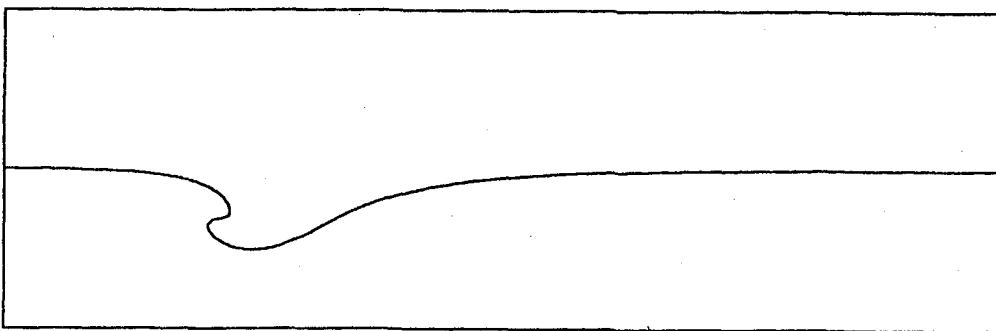
(c) Density interface.

Figure 15.—Stratified starting shear layer - ∇_ϕ = u$_{ave}$ at t = 1.44.
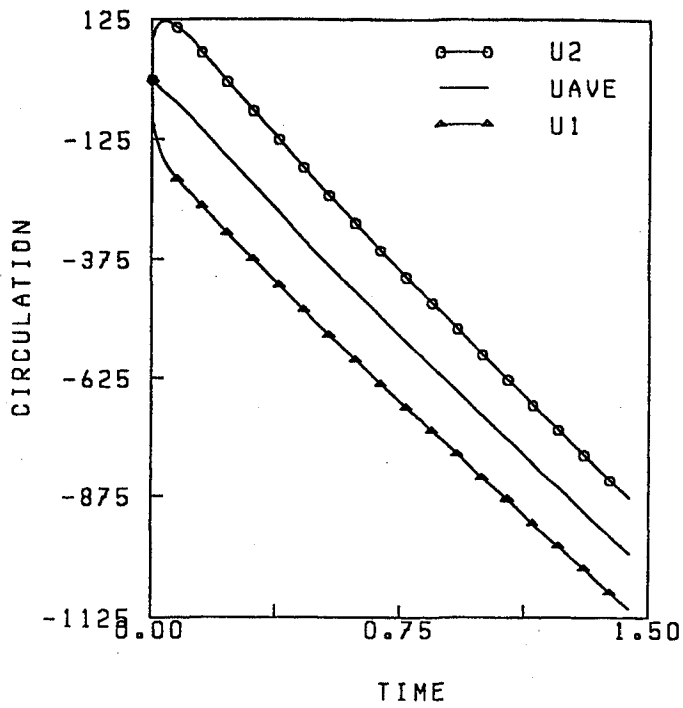
Figure 16.—Circulation history: stratified starting shear layers.
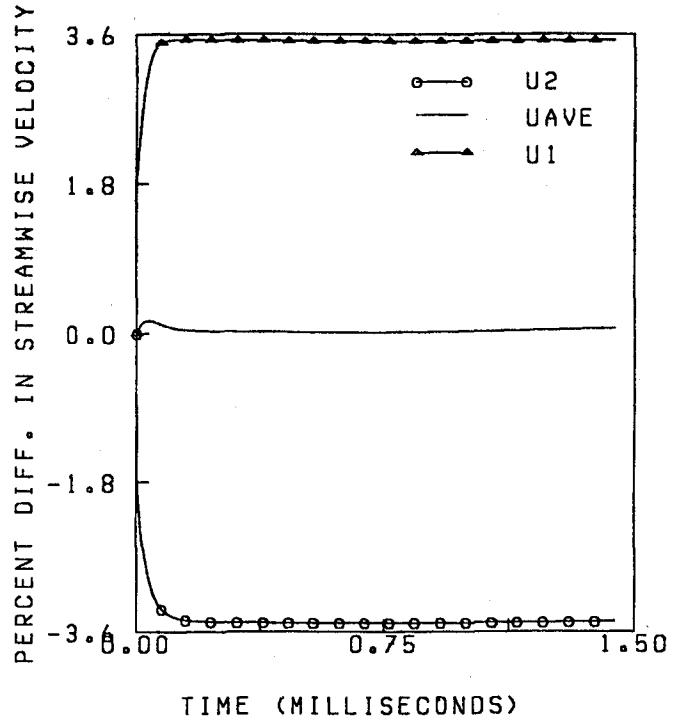
Figure 17.—Streamwise velocity difference: stratified starting shear layers.
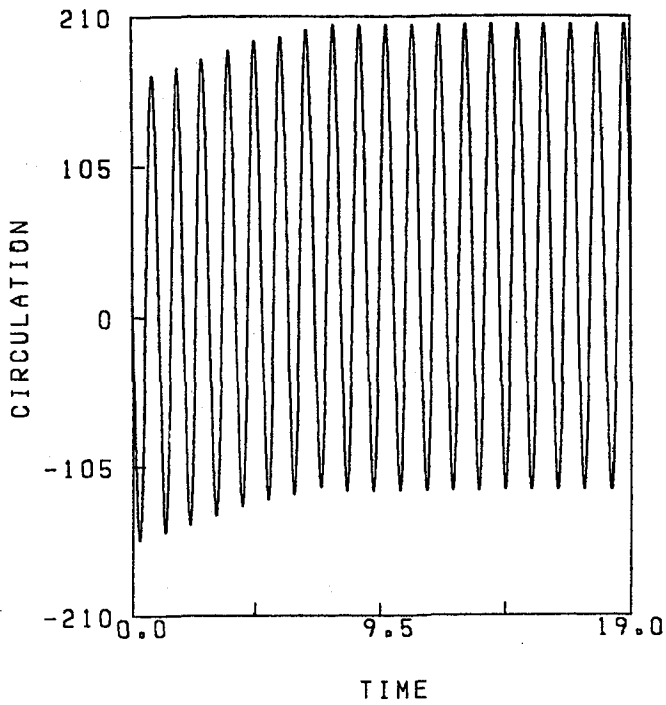
Figure 18.—Circulation history: oscillating irrotational inflow.
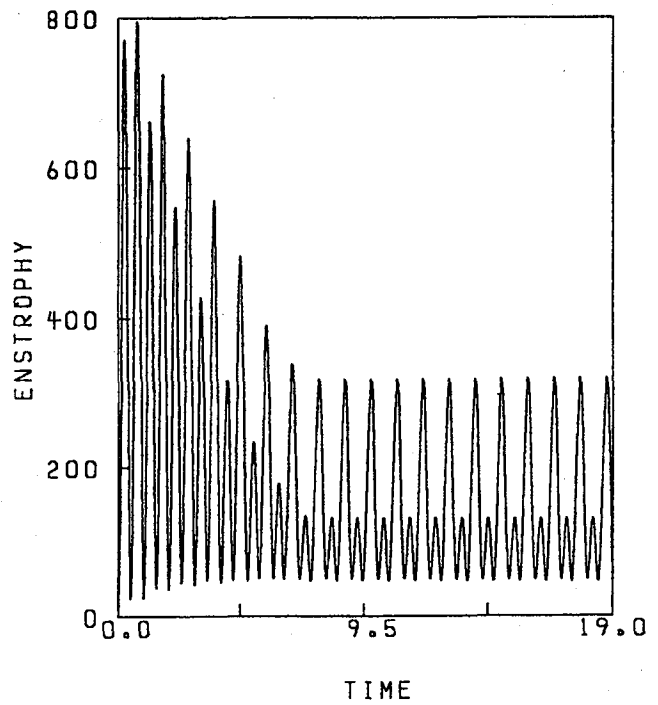
Figure 19.—Enstrophy history: oscillating irrotational inflow.

51
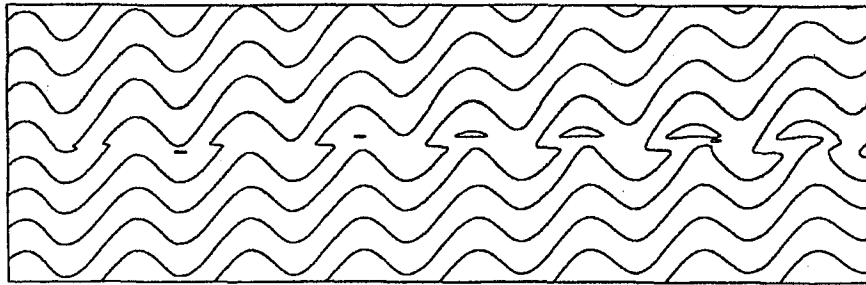
MIN= -1.5418   MAX=   -1.2408   INC=   0.0188
PHI CONTOURS

(a) $\tilde{\omega}$ t = 45°.
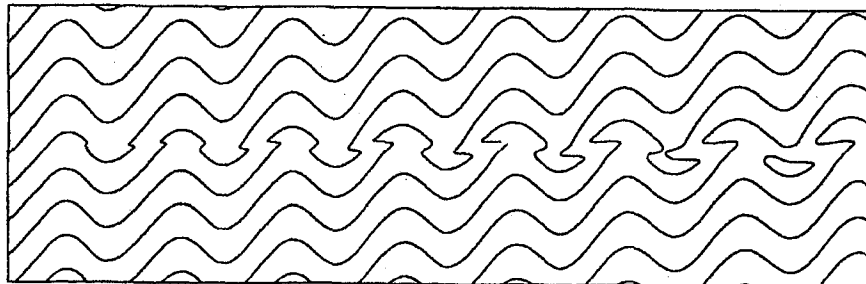
MIN= -1.5758   MAX=   -1.2560   INC=   0.0200
PHI CONTOURS

(b) $\tilde{\omega}$t = 135°.
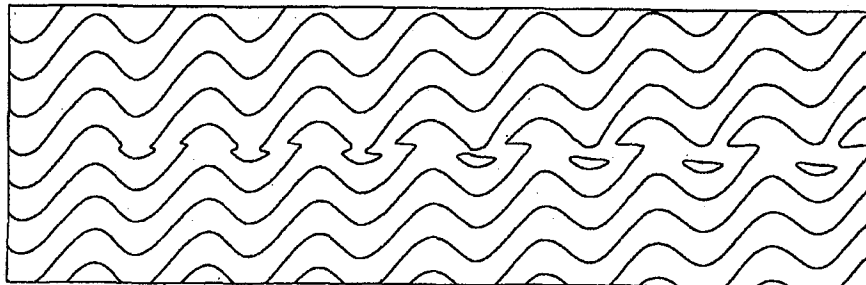
MIN= -1.5994   MAX=   -1.2768   INC=   0.0202
PHI CONTOURS

(c) $\tilde{\omega}$t = 225°.
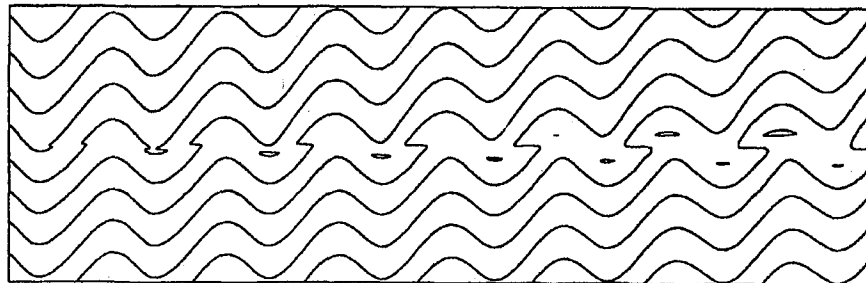
MIN= -1.6164   MAX=   -1.3018   INC=   0.0197
PHI CONTOURS

(d) $\tilde{\omega}$t = 315°.

Figure 20.—Φ potential field: oscillating irrotational inflow.
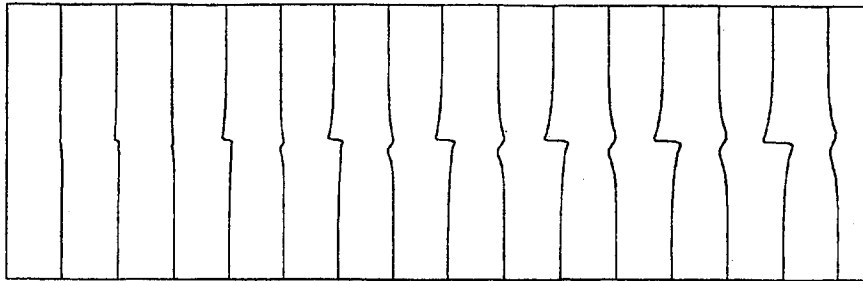
MIN= -1.6451   MAX=   -1.3306   INC=   0.0197
X CONTOURS

(a) $\tilde{\omega} t = 45°$.
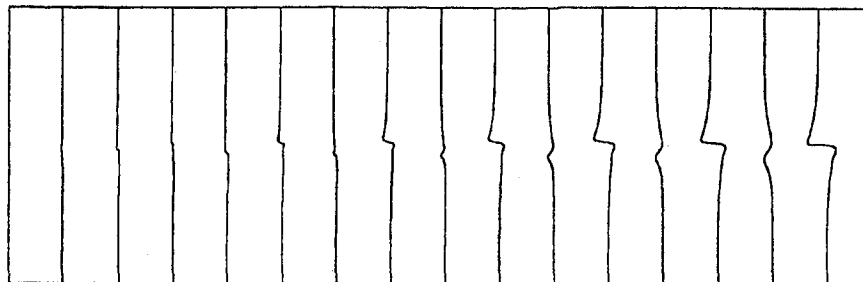
MIN= -1.6596   MAX=   -1.3489   INC=   0.0194
X CONTOURS

(b) $\tilde{\omega} t = 135°$.
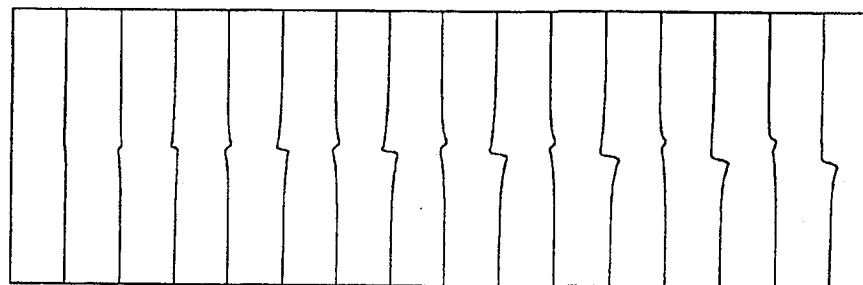
MIN= -1.6701   MAX=   -1.3590   INC=   0.0194
X CONTOURS

(c) $\tilde{\omega} t = 225°$.
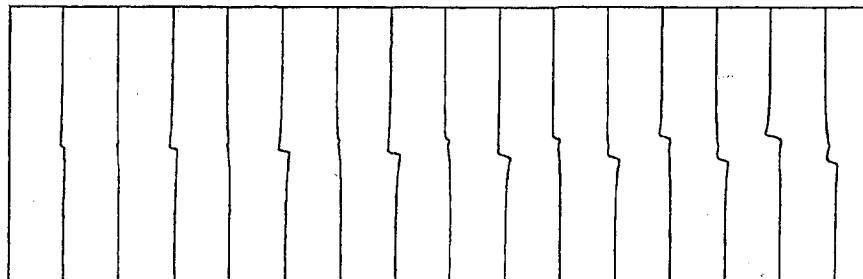
MIN= -1.6756   MAX=   -1.3619   INC=   0.0196
X CONTOURS

(d) $\tilde{\omega} t = 315°$.

Figure 21.—Φ material field: oscillating irrotational inflow.
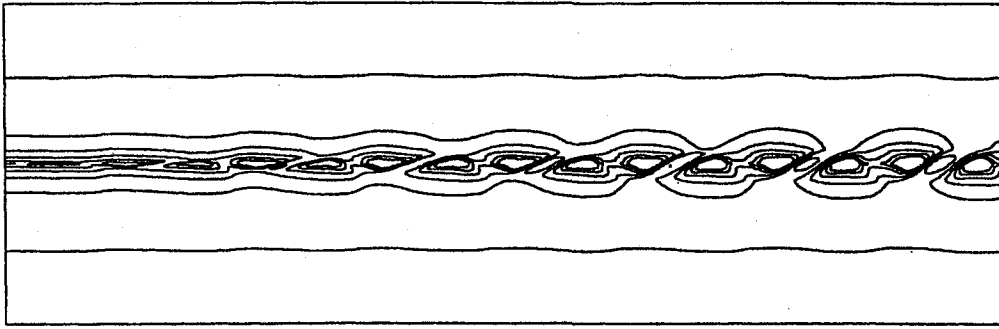
```
MIN =   0.955E 00     MAX = 0.800E 01    INC = 0.141E 01
        STREAMWISE GRADIENT OF X                    (
```

Figure 22.—Streamwise gradient of the X material field at $\tilde{\omega}t = 135°$: oscillating irrotational inflow.
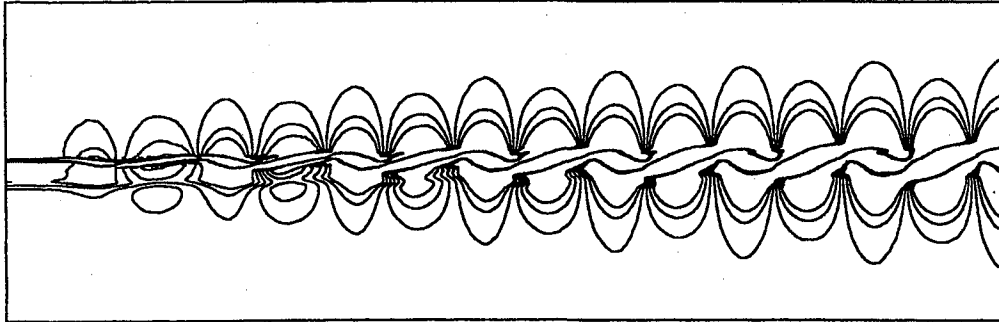

```
MIN =  -0.902E-01     MAX = 0.682E-01    INC = 0.317E-01
        CROSS-STREAM GRADIENT OF X
```

Figure 23.—Cross-stream gradient of the X material field at $\tilde{\omega}t = 135°$: oscillating irrotational inflow.
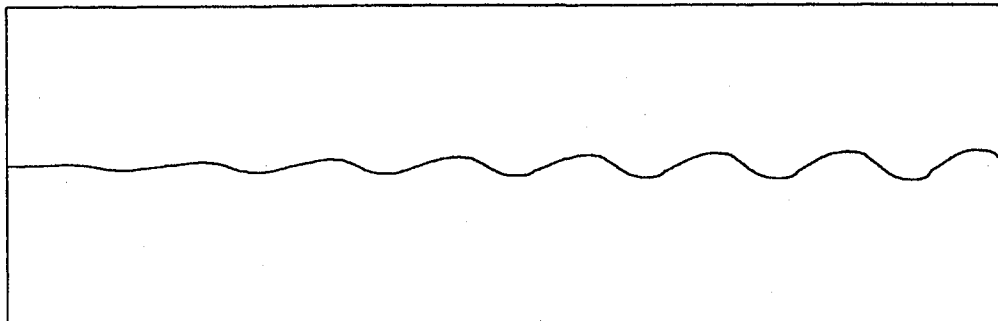
Figure 24.—Density interface at $\tilde{\omega}t = 135°$: oscillating irrotational inflow.
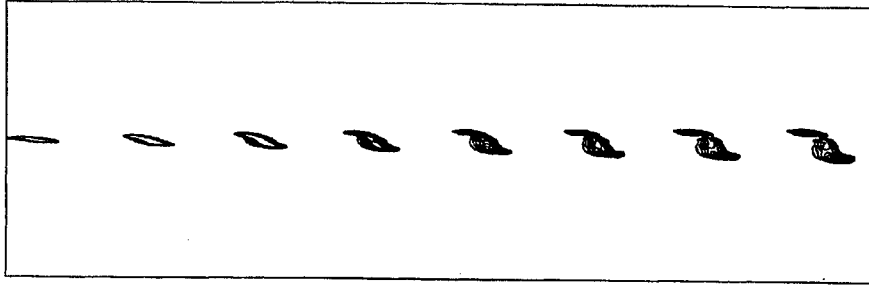
MIN = -0.473E 02   MAX = 0.287E 00   INC = 0.476E 01
VORTICITY CONTOURS

(a) $\tilde{\omega}t = 18°$.
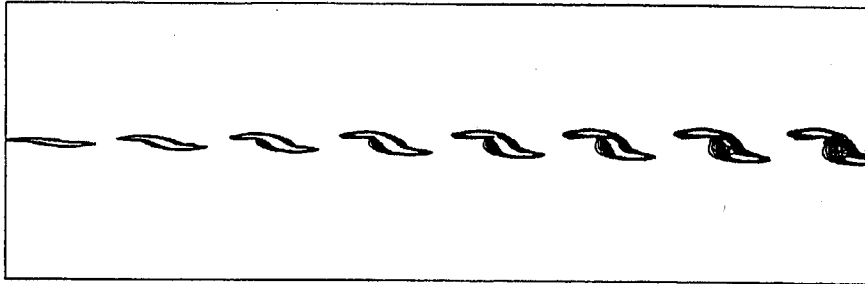
MIN = -0.425E 02   MAX =   0.000   INC = 0.425E 01
VORTICITY CONTOURS

(b) $\tilde{\omega}t = 63°$.
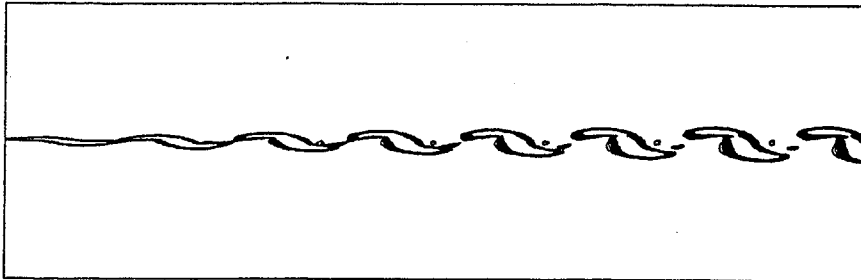
MIN = -0.224E 02   MAX =   0.000   INC = 0.224E 01
VORTICITY CONTOURS

(c) $\tilde{\omega}t = 99°$.
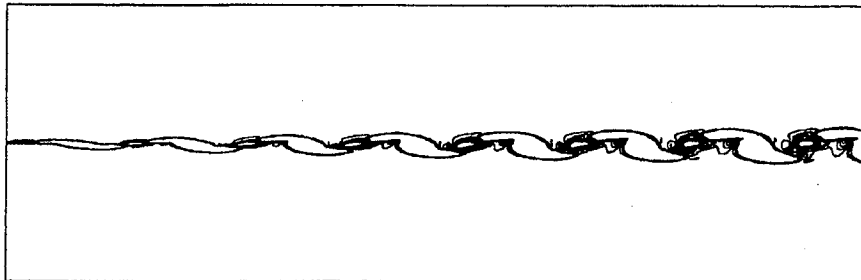
MIN = -0.371E 01   MAX = 0.893E 01   INC = 0.126E 01
VORTICITY CONTOURS

(d) $\tilde{\omega}t = 126°$.

Figure 25.—Vorticity: oscillating irrotational inflow.

55
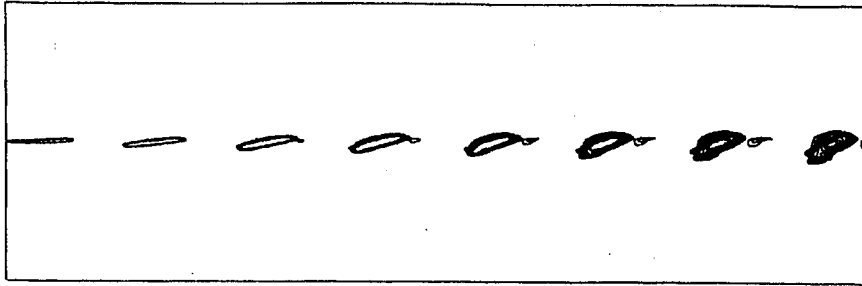
MIN = 0.000   MAX = 0.323E 02   INC = 0.323E 01
VORTICITY CONTOURS

(e) $\tilde{\omega}t = 171°$.
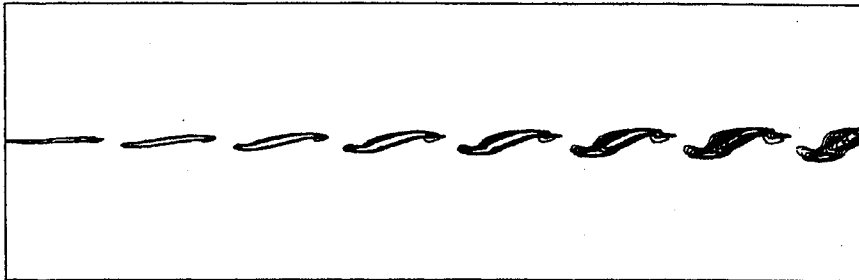
MIN = 0.000   MAX = 0.713E 02   INC = 0.713E 01
VORTICITY CONTOURS

(f) $\tilde{\omega}t = 216°$.
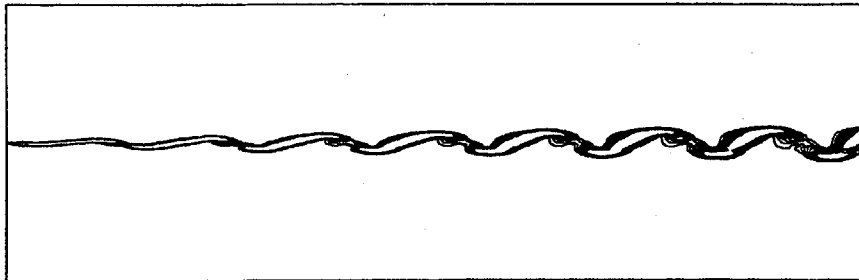
MIN = 0.000   MAX = 0.545E 02   INC = 0.545E 01
VORTICITY CONTOURS

(g) $\tilde{\omega}t = 279°$.
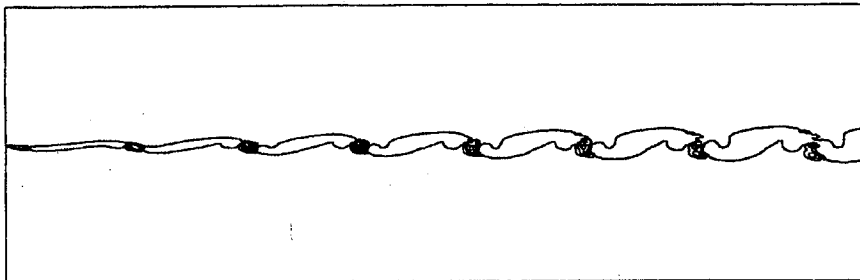
MIN = -0.265E 02   MAX = 0.506E 01   INC = 0.316E 01
VORTICITY CONTOURS

(h) $\tilde{\omega}t = 333°$.

Figure 25.—Concluded.

56
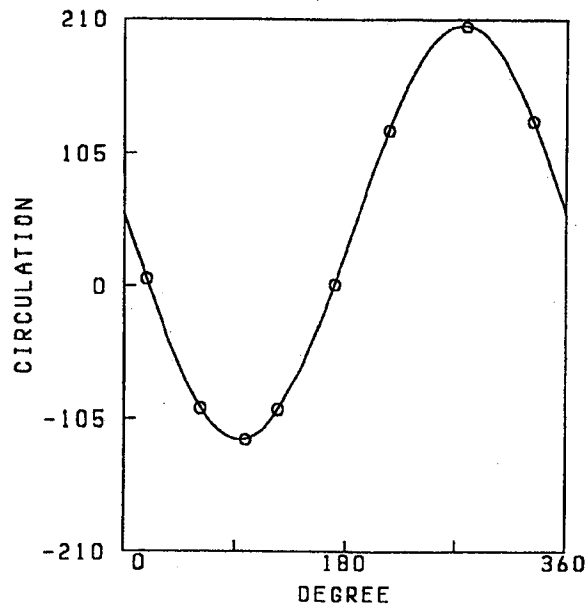
Figure 26.—One period of the circulation history.
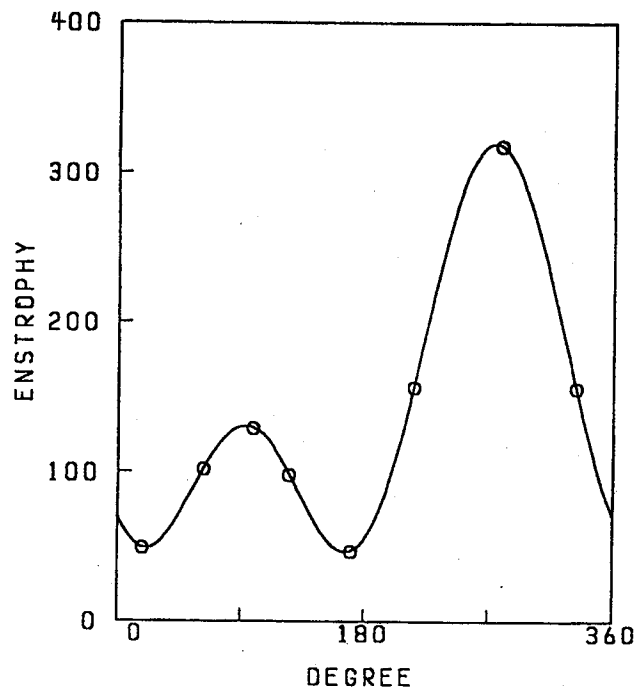
Figure 27.—One period of the enstrophy history.

REPORT DOCUMENTATION PAGE

Public reporting burden for this collection of information is estimated to average 1 hour per response, including the time for reviewing instructions, searching existing data sources, gathering and maintaining the data needed, and completing and reviewing the collection of information. Send comments regarding this burden estimate or any other aspect of this collection of information, including suggestions for reducing this burden, to Washington Headquarters Services, Directorate for information Operations and Reports, 1215 Jefferson Davis Highway, Suite 1204, Arlington, VA 22202-4302, and to the Office of Management and Budget, Paperwork Reduction Project (0704-0188), Washington, DC 20503.

1. AGENCY USE ONLY (Leave blank)	2. REPORT DATE	3. REPORT TYPE AND DATES COVERED
	October 1992	Final Contractor Report

4. TITLE AND SUBTITLE

Unsteady Shear Disturbances Within a Two-Dimensional Stratified Flow

5. FUNDING NUMBERS

6. AUTHOR(S)

Jeffrey W. Yokota

7. PERFORMING ORGANIZATION NAME(S) AND ADDRESS(ES)

Sverdrup Technology, Inc.
Lewis Research Center Group
2001 Aerospace Parkway
Brook Park, Ohio   44142

8. PERFORMING ORGANIZATION REPORT NUMBER

None

9. SPONSORING/MONITORING AGENCY NAMES(S) AND ADDRESS(ES)

National Aeronautics and Space Administration
Lewis Research Center
Cleveland, Ohio 44135-3191

10. SPONSORING/MONITORING AGENCY REPORT NUMBER

NASA CR-189121

11. SUPPLEMENTARY NOTES

12a. DISTRIBUTION/AVAILABILITY STATEMENT

Unclassified - Unlimited
Subject Category 34

12b. DISTRIBUTION CODE

13. ABSTRACT (Maximum 200 words)

The origin and evolution of shear disturbances within a stratified, inviscid, incompressible flow are investigated numerically by a Clebsch/Weber decomposition-based scheme. In contrast to homogeneous flows, within which vorticity can be redistributed but not generated, the presence of a density stratification can render an otherwise irrotational flow vortical. In this work a kinematic decomposition of the unsteady Euler equations separates the unsteady velocity field into rotational and irrotational components. The subsequent evolution of these components is used to investigate the influence various velocity disturbances have on both stratified and homogenous flows. In particular, the flow within a two-dimensional channel is used to investigate the evolution of rotational disturbances, generated or convected, downstream from an unsteady inflow condition. Contrasting simulations of both stratified and homogeneous flows are used to distinguish between redistributed inflow vorticity and that which is generated by a density stratification.

14. SUBJECT TERMS

Inviscid flow; Shear layers; Vortex sheets

15. NUMBER OF PAGES

58

16. PRICE CODE

A04

17. SECURITY CLASSIFICATION OF REPORT	18. SECURITY CLASSIFICATION OF THIS PAGE	19. SECURITY CLASSIFICATION OF ABSTRACT	20. LIMITATION OF ABSTRACT
Unclassified	Unclassified	Unclassified	

National Aeronautics and
Space Administration

Lewis Research Center
Cleveland, Ohio 44135

Official Business
Penalty for Private Use $300

NASA